the received signals $\mathbf{Y}$ with the channel response $\mathbf{H}$. We show how to calculate APP using the BCJR algorithm [14] as follows. From the received signal $\sum_{\nu=1}^{N_r} y_n^\nu(p)$ and the *a-priori probability* $P(\tilde{x}_n^\mu(p))$, the $\gamma_p^i(s_{p-1}^i, s_p^i)$ value is computed as follows:

$$\gamma_p^i(s_{p-1}^i, s_p^i) = P(\tilde{x}_n^\mu(p)) \times \frac{1}{\sqrt{2\pi\sigma^2}} \exp\left\{-\frac{1}{2\sigma^2}|d_{free}(n,p)|^2\right\} \tag{14}$$

where σ^2 is the variance of AWGN ($= N_r N_0$) and $d_{free}(n,p)$ is defined as

$$d_{free}(n,p) = \sum_{\nu=1}^{N_r} y_n^\nu(p) - \sum_{\nu=1}^{N_r}\sum_{\mu=1}^{N_t} H_{\mu\nu}^n(p)\tilde{x}_n^\mu(p). \tag{15}$$

$\tilde{x}_n^\mu(p)$ shows the estimated symbol at the μth transmit antenna, pth subcarrier and nth symbol. Utilizing $\gamma_p^i(s_{p-1}^i, s_p^i)$, the values of $\alpha_p^i(s_p^i)$ and $\beta_{p-1}^i(s_{p-1}^i)$ and the APP are computed as follows:

$$\alpha_p^i(s_p^i) = \sum_{s_{p-1}} \gamma_p^i(s_{p-1}^i, s_p^i) \cdot \alpha_{p-1}^i(s_{p-1}^i) \tag{16}$$

$$\beta_{p-1}^i(s_{p-1}^i) = \sum_{s_p} \gamma_p^i(s_{p-1}^i, s_k^i) \cdot \beta_p^i(s_p^i) \tag{17}$$

$$\Pr(\tilde{S}_n(p) = a) = \sum_{\tilde{S}_n(p)=a} \gamma_p^i(s_{p-1}^i, s_p^i)\alpha_{p-1}^i(s_{p-1}^i)\beta_p^i(s_p^i). \tag{18}$$

The symbol a shows the symbol index, e.g., the symbol a is chosen from the symbol index $[0, 1, 2, 3]$ in the case of QPSK modulation. s_p^i shows the trellis state index of the inner code at the pth time slot. The results of the SISO MAP decoder of SF code are transformed to binary probability from the symbol domain probability as follows:

$$\Pr(\tilde{b'}_c(k,p) = 1) = \sum_{\tilde{b'}_c(k,p)=1} \Pr(\tilde{S}_n(p)) \tag{19}$$

$$\Pr(\tilde{b'}_c(k,p) = 0) = \sum_{\tilde{b'}_c(k,p)=0} \Pr(\tilde{S}_n(p)) \tag{20}$$

where $\tilde{b'}_c(k,p)$ is the kth estimated binary data on the pth subcarrier ($k \in [1, 2, \cdots, K]$, $K = N_s \log_2 |\mathcal{A}_X|$). The results which are transformed to binary probabilities are deinterleaved as follows:

$$\pi^{-1} : \Pr(\tilde{\mathbf{b}}'_c) \to \Pr(\tilde{\mathbf{b}}_c). \tag{21}$$

The deinterleaved binary probabilities are then considered as the inputs to the SISO MAP decoder of the outer (channel) code. We show how to calculate the LLR of the outer code with the BCJR algorithm [14], [19]. The *a priori probabilities* of the outer code are always a constant values ($\Pr(b_i(k,p)) = \frac{1}{2}$). Then, we can write the branch metric $\gamma_k^o(s_{k-1}^o, s_k^o)$ with the input bit probabilities $\Pr(\tilde{\mathbf{b}}_c)$ as

$$\begin{aligned}\gamma_k^o(s_{k-1}^o, s_k^o) &= \frac{\Pr(s_{k-1}^o, s_k^o, \Pr(\tilde{\mathbf{b}}_c))}{\Pr(s_{k-1}^o)} \\ &= \left[\frac{\Pr(s_{k-1}^o, s_k^o)}{\Pr(s_{k-1}^o)}\right]\left[\frac{\Pr(s_{k-1}^o, s_k^o, \Pr(\tilde{\mathbf{b}}_c))}{\Pr(s_{k-1}^o, s_k^o)}\right] \\ &= \Pr(s_k^o|s_{k-1}^o)\Pr(\Pr(\tilde{\mathbf{b}}_c)|s_{k-1}^o, s_k^o) \\ &= \Pr(b_i(k,p))\Pr(\Pr(\tilde{\mathbf{b}}_c)|s_{k-1}^o, s_k^o).\end{aligned} \tag{22}$$

The $\alpha_k^o(s_k^o)$ value, $\beta_{k-1}^o(s_{k-1}^o)$ value and log-likelihood *a posteriori* value can be expressed as

$$\alpha_k^o(s_k^o) = \sum_{s_{k-1}^o} \gamma_k^o(s_{k-1}^o, s_k) \cdot \alpha_{k-1}^o(s_{k-1}^o) \tag{23}$$

$$\beta_{k-1}^o(s_{k-1}^o) = \sum_{s_k^o} \gamma_k^o(s_{k-1}^o, s_k^o) \cdot \beta_k^o(s_k^o) \tag{24}$$

$$\begin{aligned}&\Lambda(b_i(k,p)|\Pr(\tilde{\mathbf{b}}_c)) \\ &= \ln\frac{\Pr(b_i(k,p) = +1|\Pr(\tilde{\mathbf{b}}_c))}{\Pr(b_i(k,p) = 0|\Pr(\tilde{\mathbf{b}}_c))} \\ &= \ln\frac{\sum_{\tilde{b}_i(k,p)=+1}\gamma_k^o(s_{k-1}^o, s_k^o)\alpha_{k-1}^o(s_{k-1}^o)\beta_k^o(s_k^o)}{\sum_{\tilde{b}_i(k,p)=0}\gamma_k^o(s_{k-1}^o, s_k^o)\alpha_{k-1}^o(s_{k-1}^o)\beta_k^o(s_k^o)}\end{aligned} \tag{25}$$

$$\begin{aligned}&\Lambda(b_c(k,p)|\Pr(\tilde{\mathbf{b}}_c)) \\ &= \ln\frac{\Pr(b_c(k,p) = +1|\Pr(\tilde{\mathbf{b}}_c))}{\Pr(b_c(k,p) = 0|\Pr(\tilde{\mathbf{b}}_c))} \\ &= \ln\frac{\sum_{\tilde{b}_c(k,p)=+1}\gamma_k^o(s_{k-1}^o, s_k^o)\alpha_{k-1}^o(s_{k-1}^o)\beta_k^o(s_k^o)}{\sum_{\tilde{b}_c(k,p)=0}\gamma_k^o(s_{k-1}^o, s_k^o)\alpha_{k-1}^o(s_{k-1}^o)\beta_k^o(s_k^o)}\end{aligned} \tag{26}$$

where $b_i(k,p)$ and $b_c(k,p)$ show the information and coded data at the pth subcarrier and kth symbol interval [19]. Λ shows the LLR of the outer code. In order to obtain the *a priori probability* of the inner code, we subtract the *a priori probability* and the channel value from Λ. In the case of the outer code, we define the LLRs of *a priori* values as zero. Therefore, we subtract only the channel value from Λ. The results of the subtraction are interleaved. The interleaved results are transformed to symbol domain probabilities ($P(\tilde{x}_n^\mu(p))$). The symbol domain probabilities are considered as the *a priori probability* for the inner code (SF code). Using this calculated *a priori probability* of the inner codes, we decode the signals once more. If the number of iterations is less than a maximum number allowed, we compare the APP of the outer code with zero.

4. Evaluations

In this section, we evaluate the proposed system. Consider that the channel model in this evaluation is a time-varying and frequency-selective Rayleigh fading channel where the center frequency is 1 GHz, the bandwidth is 1 MHz and one OFDM frame consists of 128 sub-carriers and 100 symbols. For the sake of simplicity, we assume that each path from each transmit antenna to each receive antenna is independent. We assume that the channel gain is constant for one

symbol and one subcarrier interval. Consider the case of a 2-transmit, 1-receive antenna and QPSK transmission system. In the case of optimization of SF (or ST) code, the way of code design criterion depends on the achievable diversity gain (i.e., the number of transmit/receive antennas) [8], [9]. In order to optimize a turbo system, we should investigate the weight distribution, minimum free distance, interleaver design and so on [12], [15], [18]. Here, we focus on not the optimization of SF code but the optimization of the kind of each element code. Then, we assume the simplest multi-input single-output (MISO) channel. In this section, we evaluate the BER performance with computer simulations.

4.1 Evaluation of the Inner Code

In this subsection, we evaluate the inner code. Figure 4 shows the non-recursive [5] and recursive [6] 4-state QPSK 2 transmit space-frequency trellis diagrams. The states displayed in the diagram follow the patterns given by $[S(p)/S_1(p), S_2(p)]$. $S(p)$ is the input symbol of pth subcarrier and $S_\mu(p)$ shows the transmit symbol of $p$the subcarrier from μth transmit antenna. Figure 5 shows the comparison between the case that the inner encoder is a non-recursive space-frequency (non-RSF) code and the case where it is a recursive space-frequency (RSF) code. The kind of interleaver between the inner encoder and the outer encoder is a random interleaver. In both cases, we use the 7-5 non-recursive convolutional (non-RC) code ($R_{ch} = 1/2$) as an outer code. Obviously, the element encoders and interleaver used in this paper are not optimum for the STF turbo code. In this paper, we aim to design the optimum structure of STF turbo code in order to obtain the diversity gain over space, time and frequency effectively. Then, we use a simple code for the optimization of structure of STF turbo code. We assume that the channel model is the time-varying and frequency-selective channel with the Doppler frequency 100 Hz and delay spread 1 μsec. From Fig. 5, it is seen that the better structure for inner encoder is of recursive type. N_{iter} shows the number of iterations. The performance of the concatenation between non-RSF and non-RC codes can not obtain an interleaver gain. From [12], in contrast with the case of a non-recursive inner encoder, the use of a recursive inner encoder yields an interleaver gain. As a consequence, the inner encoder must be a recursive encoder. From the comparison of BER performances between 9 and 10 iterations, there is negligible improvement. Then we can assume that the performance of the concatenation between RSF and non-RC codes can not achieve higher gain in the case of more than 9 iterations. Hereinafter, we use the RSF code as an inner code and evaluate the systems using 9 iterations.

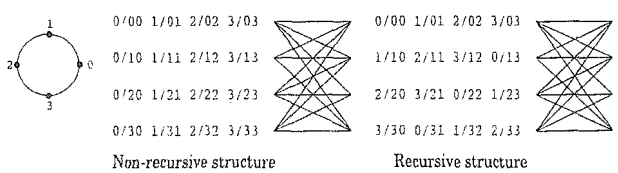

Fig. 4 Trellis diagram for 2-transmit 4-state QPSK non-recursive/recursive space-frequency code.

4.2 Evaluation of the Outer Code

In this subsection, we evaluate the outer code. Consider that the inner code is the RSF code and the interleaver between each code is a random interleaver. We evaluate three cases, first, the outer code is a 7-5 non-RC code ($R_{ch} = 1/2$), second, the outer code is a 7-5 recursive systematic convolutional (RSC) code ($R_{ch} = 1/2$), and third, the outer code is a turbo code ($R_{ch} = 1/2$) which is punctured and consists of two 7-5 RSC codes ($R = 1/2$) and a random interleaver. Figure 6 shows the decoder structure in the case that the outer code is a turbo code. π_1 shows the interleaver function for concatenation between inner and outer codes. π_2 shows the interleaver function for the outer turbo code. In the decoding process of concatenation between RSF and turbo codes, we have the iterative decoding techniques of the time-frequency domain turbo code and the concatenation between the RSF (inner) code and turbo (outer) codes. We briefly explain the decoding process of the concatenation between the RSF (inner) code and turbo (outer) codes. The inner decoder computes the LLRs from the received signals. The results of inner decoding are deinterleaved and are considered as the inputs of the outer decoder. The outer decoder of the TF domain turbo code computes the LLRs with several iterations. After several iterative decoding of the turbo (outer) code, the results are interleaved and go to the inner decoder as the *a priori probability*. In one decoding cycle, there are the MAP decoding of inner code and the turbo decoding of outer code. The computational complexity of the concatenation between RSF and turbo codes is much higher than that of the concatenation between RSF and non-RC (or RSC) codes. We describe the computational complexity in Sect. 6.

Figure 7 shows the comparison between three cases

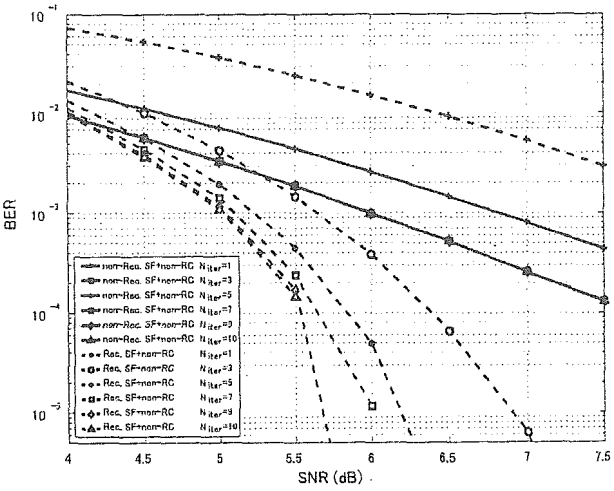

Fig. 5 BER performance in the cases that the inner encoder is of recursive or non-recursive type.

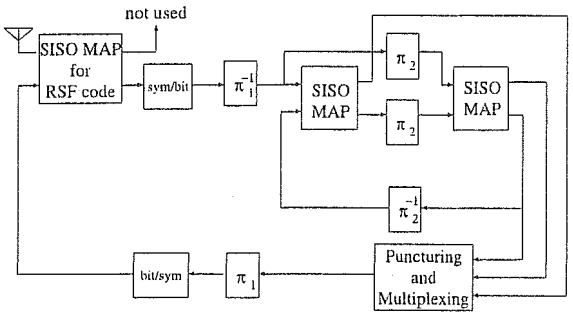

Fig. 6 Decoding structure in the case that the outer code is a turbo code.

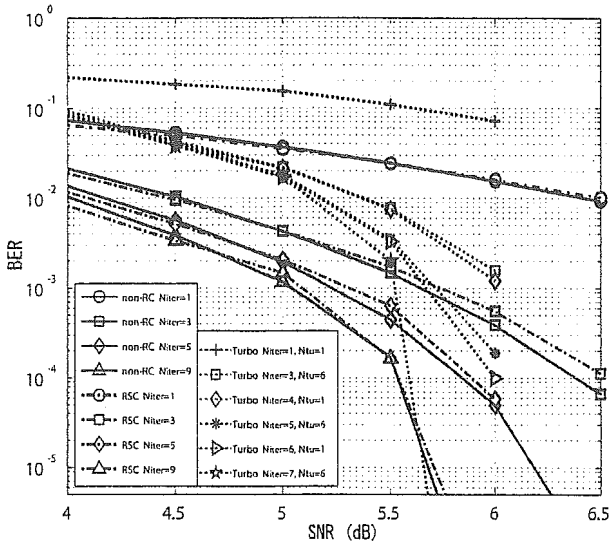

Fig. 7 BER performance in the cases that the outer code is the non-RC, RSC and turbo codes.

where the Doppler frequency is 100 Hz and the delay spread is 1 μsec. N_{Tu} shows the number of iterations for the turbo (outer) code. Due to high computational complexity, we consider that the maximum number of N_{Tu} and N_{iter} are 6 and 7 times respectively in the case that the outer code is turbo code. We evaluate the performance at 10^{-5} BER. In this case, the concatenation between RSF and turbo codes has slightly better performance than the other two codes. However, the concatenation between RSF and turbo codes has much higher computational complexity than the other two concatenated codes. In this paper, the error floor is not evaluated, since the region of error floor is very low BER in the case of serial concatenated code [12]. In the case that the outer code is turbo code, it is seen from the comparison between the case of $N_{iter}/N_{tu} = 6/1$ and the case of $N_{iter}/N_{tu} = 5/6$ that the amount of improvement due to iteration between SF and TF codes is low. Then, the performance of the concatenation between RSF and turbo codes depends on the effect of not the concatenation between SF (=RSF) and TF (=turbo) codes but the TF domain (turbo) code. On the other hand, the performances of the concatenation between RSF and non-RC/RSC codes depend on

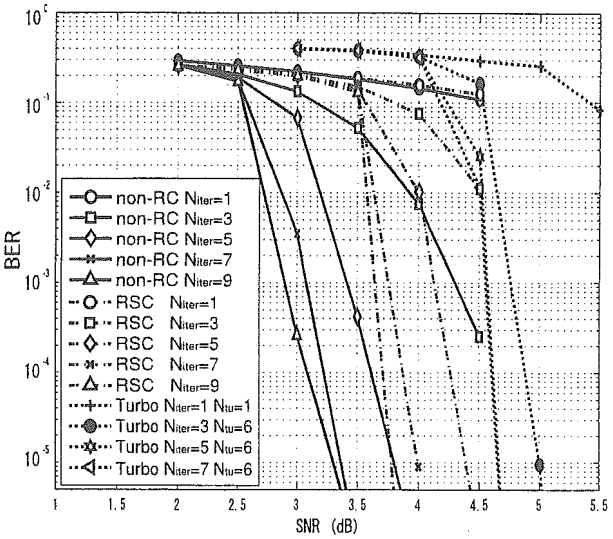

Fig. 8 BER performance in the cases that the outer code is a RSC and non-RC and turbo code and that the inner code is a recursive space-frequency code.

the effect of the concatenation between SF (=RSF) and TF (=nonRC/RSC) domain codes. From the comparison between the cases of nonRC code and RSC code, it is seen that the performance of nonRC achieve slightly better than that of RSC. As described in [12], the outer code should be a non-recursive code with large free distance in order to provide a large interleaver gain. The reason can be considered as same reason of reference [12].

In order to obtain maximum diversity gain over STF domain and interleaver gain between SF and TF codes, we interleave the encoded signals before transmitting. We assume that this interleaver is ideal. Therefore, we can consider that the channel response of each signal and each carrier is independent. Figure 8 shows the BER performances in the case that the outer code is non-RC, RSC and turbo codes where the channel response of each symbol and carrier is independent. It is seen from Fig. 8 that the concatenation between RSF and non-RC codes has better performance than the other codes. The outer code should be of a non-recursive code with a large free distance [12]. Then, the cases of non-RC and RSC have better performance than the case of turbo code. Comparing between the non-RC and the RSC codes, the free distance of both cases is same. The difference between non-RC and RSC is the amount of maximum input weight ($w_{non-RC} = 1$, $w_{RSC} = 2$) [19]. Then, the performance of non-RC code is better than that of RSC. Therefore, the best structure of outer code is of a non-RC type in order to achieve the highest coding gain.

5. Analysis Using EXIT Chart

In this section, we analyze the optimum structure of inner/outer codes with EIXT chart.

5.1 EIXT Chart

EXIT chart have been proposed for the analysis of convergence behavior of iterative processing [16], [17]. EXIT analysis is the chart which expresses a variation of the mutual information. Using EXIT chart analysis for iterative processing (e.g., turbo code, LDPC code, turbo equalizer and so on), the convergence behavior can be analyzed with reasonable computational complexity. In order to apply EXIT chart to the analysis of turbo code, the turbo decoder is divided into each element decoder. Each element decoder computes the mutual information of extrinsic information with several *a priori* values. The results calculated by each decoder are depicted in the same figure. This figure is corresponding to the convergence behavior of iterative processing.

The aim of this analysis in this section is that the best structure of inner/outer codes is chosen. The structure of inner code must be of a recursive type [12]. Then, we evaluate only the kind of outer code.

5.2 Iterative Decoding Process

In this subsection, we show the relation between each log likelihood ratios (LLRs) $Z_i, A_i, E_i, D_i, Z_o, A_o, E_o, D_o$. Z_i, A_i, E_i and D_i show the LLR for channel value, *a priori* value, *extrinsic* value and *a posteriori* value in the case of inner decoding, respectively (Fig. 9). Z_o, A_o, E_o, D_o show the LLR for channel value, *a priori* value, *extrinsic* value and *a posteriori* value in the case of outer decoding, respectively (Fig. 10).

First, the decoder decodes the received signals with the symbol-symbol MAP algorithm in order to compute the symbol domain *a posteriori* value D'_i. The symbol domain *a posteriori* value D'_i is transformed into the bit domain *a posteriori* value D_i. Then the *a posteriori* value D_i is given by

$$D_i = Z_i + A_i + E_i \tag{27}$$

where Z_i is the bit domain LLR. Second, the inner decoder subtracts the only *a priori* value A_i from D_i. This process is a common decoding scheme in the case of a serial concatenated convolutional code [12], [13], [16]. The result $(D_i - A_i = Z_i + E_i)$ is deinterleaved and goes to the outer decoder as the input value Z_o $(= \pi^{-1}(Z_i + E_i))$. Note that the amount of mutual information is invariant after interleaving (deinterleaving). Third, the outer decoder calculates the *a posteriori* value D_o with the channel value Z_o and *a priori* value A_o. In the case of a serial concatenated convolutional code, the *a priori* value of outer decoder A_o is zero at any iteration. Then, the *a posteriori* value D_o is given by

$$D_o = Z_o + A_o + E_o = Z_o + E_o. \tag{28}$$

In order to calculate the *extrinsic* value E_o, the decoder subtracts the channel value Z_o from D_o. This *extrinsic* value E_o is interleaved and becomes the *a priori* value A_i of inner code as follows:

$$A_i = \pi(D_o - Z_o) = \pi(E_o). \tag{29}$$

This is one decoding cycle. The decoder can decode iteratively with this cycle. We describe the detailed way to compute the mutual information in the latter subsection.

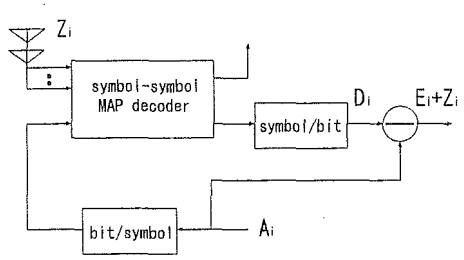

Fig. 9 Structure of inner decoder.

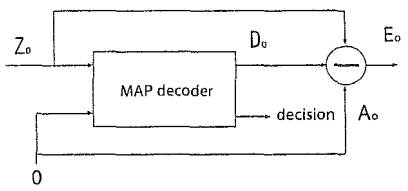

Fig. 10 Structure of outer decoder.

5.3 EXIT Characteristic of Inner Code

At first we describe the inner code that is a space-frequency code. Figure 9 shows the structure of decoder in order to calculate the mutual information. We consider the bit domain analysis. The inner code is the symbol domain SISO decoder, then we transform from the symbol domain to the bit domain mutual information. Figure 9 shows the SISO decoder in order to calculate the bit domain mutual information. The bit domain probability can be calculated with Eqs. (19) and (20).

In the decoding process, the *a priori* values are transformed from the bit domain values $P_a(b_c)$ to symbol domain values $P_a(s)$ as following

$$\begin{aligned} P_a(b_c = 1) &= \frac{\exp(A_i)}{1 + \exp(A_i)} \\ P_a(b_c = 0) &= \frac{1}{1 + \exp(A_i)} \\ P_a(s) &= \prod_{k=1,2,\cdots K} P_a(b_c = b'') \\ K &= \log_2 |\mathcal{A}_X|, b'' \in \{0, 1\}. \end{aligned} \tag{30}$$

With the received signals and the symbol domain *a priori* probabilities, the symbol-symbol SISO decoder can calculate the *a posteriori* values D'_i. D'_i is transformed to bit domain *a posteriori* values D_i. In order to calculate the extrinsic values, the calculated *a posteriori* values D_i are subtracted only by the *a priori* values A_i $(D_i - A_i = Z_i + E_i)$.

Z_i is the function of SNR. Viewing $I_{E_i+Z_i}$ (mutual information of the output) as a function of I_{A_i} (mutual information of *a priori* values) and the SNR value, the output information characteristics are defined as

$$I_{E_i+Z_i} = T(I_{A_i}, SNR) \tag{31}$$

or, for fixed SNR, just

$$I_{E_i+Z_i} = T(I_{A_i}) \tag{32}$$

since the MAP decoder calculate the output value $(E_i + Z_i)$ using the two input value (*a priori* value A_i and channel value Z_i). However, we can not calculate the mutual information of output value $I_{E_i+Z_i}$ with I_{A_i} and SNR, directly. Then, the mutual information of the output is used to quantify as follows:

$$I_{E_i+Z_i} = \frac{1}{2} \sum_{x=+1,-1} \int_{-\infty}^{\infty} P_{E_i+Z_i}(\xi|X = x) \times \log_2 \frac{2P_E(\xi|X = x)}{P_{E_i+Z_i}(\xi|X = -1) + P_{E_i+Z_i}(\xi|X = +1)} d\xi. \tag{33}$$

To compute $T(I_{A_i}, SNR)$ for the desired (I_{A_i}, SNR)-input combination, the distributions $P_{E_i+Z_i}$ of Eq. (33) are most conveniently determined by Monte Carlo simulation (histogram measurements) [16], [20]. Note that $P_{E_i+Z_i}$ must not be a Gaussian distribution. Figure 11 shows the pdf function of $E_i + Z_i$ of 4-state QPSK 2transmit recursive space-frequency code in the case where $I_{A_i} = 0.0, 0.3, 0.6, 0.9$, $SNR = 3$ dB. The higher I_{A_i} the decoder has, the higher $|E_i + Z_i|$ the decoder outputs. The mutual information in this EXIT chart is the bit-domain mutual information. Then the maximum mutual information is 1. The results of SISO decoder are transformed from the symbol domain values to the bit domain values and deinterleaved. The deinterleaved bit domain values become the input of the outer SISO decoder.

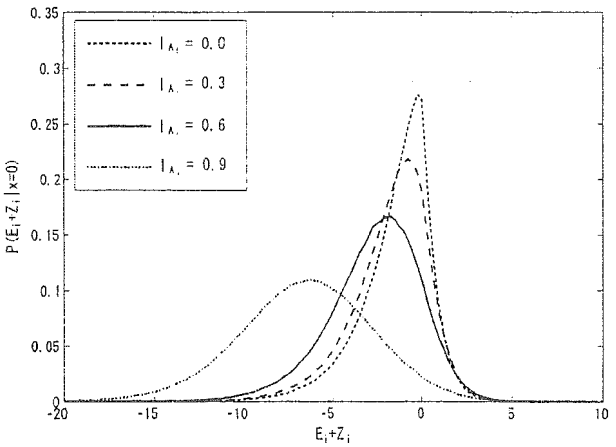

Fig. 11 The pdf function of $E_i + Z_i$ of 4-state QPSK 2transmit recursive space-frequency code in the case where $I_{A_i} = 0.0, 0.3, 0.6, 0.9$, $SNR = 3$ dB.

5.4 EXIT Characteristic of Outer Code

In this subsection, we describe the extrinsic information transfer characteristic of outer code. Figure 10 shows the structure of outer code. In the serial concatenated convolutional code, the inputs of outer code are that the values are the deinterleaved results of inner code. The *a priori* LLRs are 0 at any iteration. The function of the mutual information of extrinsic information is written as

$$I_{E_o} = T(I_{A_o}, I_{Z_o}) \tag{34}$$

where $I_{A_o} = 0$, and Eq. (34) can be transformed as

$$I_{E_o} = T(I_{Z_o}). \tag{35}$$

Therefore, the mutual information after decoding depends on the only channel values.

In order to measure the distribution P_{E_o} by Monte Carlo simulation, we assume that the channel values I_{Z_o} can be defined as Gaussian variables. Actually, the channel values I_{Z_o} are the results of inner coder. At the region of low I_{E_o}, the distribution is not a Gaussian. However, to compute I_{E_o}, we approximate the I_{Z_o} to the Gaussian distribution. Then the channel log-value is expressed as

$$\begin{aligned} Z_o &= \ln \frac{P(z|b_c = +1)}{P(z|b_c = -1)} = \frac{2}{\sigma_n^2}(x + n) \\ &= \mu_Z b_c + n_Z \end{aligned} \tag{36}$$

with

$$\begin{aligned} \mu_Z &= \frac{2}{\sigma_n^2} \\ n_Z &= \mu_Z \cdot n. \end{aligned} \tag{37}$$

n is Gaussian distributed with mean zero variance $\sigma_n^2 = N_0/2$.

With Eqs. (35) and (36), the mutual information of the extrinsic information is calculated by Monte Carlo simulation.

Solid lines in Fig. 12 show the extrinsic information transfer characteristics of the non-recursive convolutional and the turbo codes, respectively. It is seen that the performance of turbo code is worse than the convolutional code's one with the low channel value ($I_Z \leq 0.55$). On the other hand, at the high channel value region ($I_Z \geq 0.55$), the amount of turbo code's mutual information is higher. The inclination of the turbo code's performance is steeper. The reason is that the performance of the turbo code has a water fall region. Then, after the water fall, the turbo code can achieve much better performance.

5.5 EXIT Chart Analysis

In this subsection, we describe the theoretical analysis of the proposed space-time-frequency turbo code with EXIT chart. Figure 12 shows the EXIT chart of the proposed space-time-frequency turbo code. We consider two kind of outer codes.

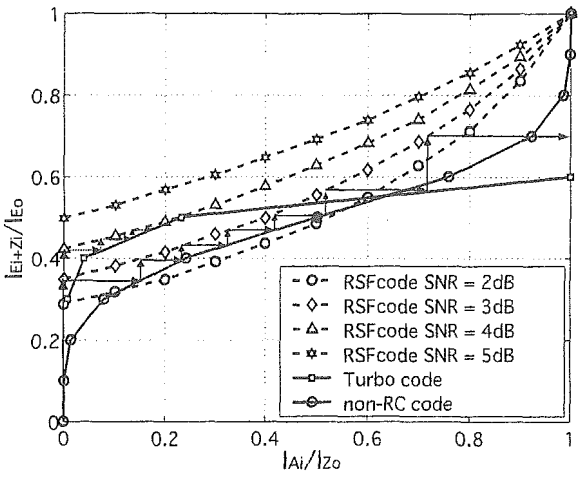

Fig. 12 Extrinsic information transfer characteristics of the proposed STF turbo code; the inner code is a 4-state RSF trellis code (2×1), the outer code is a 7-5 non-RC code and turbo code which consists of 7-5 RSC codes and a random interleaver. The coding rate of both outer codes is 1/2 (turbo code is punctured from $R = 1/3$ to $R = 1/2$).

One is a convolutional code, the other is a turbo code. The polynomial of evaluated non-RC code is (7, 5), the coding rate is 1/2. The structure of turbo code consists of two (7,5) RSC codes and the random interleaver, the coding rate is 1/2 with a puncturing technique. Recall that the aim of this evaluation is not to propose the code design criteria but to choose the best kind for the inner code. Then, in this evaluation, we use simple code.

The solid arrowhead between the solid line with circle point and the dotted line with diamond point (RSF code at SNR=3) shows the convergence behavior of iterative decoding. We describe the behavior of its arrowhead. First, the mutual information of the output value (I_{Ei+Zi}) after the inner (RSF) decoding becomes 0.35. Second, the mutual information of the *extrinsic* value (I_{Eo}) after the outer (nonRC) decoding with the input value I_{Zo} becomes 0.15. Third, the mutual information of the output value (I_{Ei+Zi}) after the inner (RSF) decoding with *a priori* information I_{Ai} becomes 0.4. Fourth, the mutual information of the *extrinsic* value (I_{Eo}) after the outer (nonRC) decoding with the input value I_{Zo} becomes 0.22. After several decoding, the mutual information becomes 1. Therefore, the performance becomes error free. On the over hand, in the case where the outer code is the turbo code, it is seen that the EXIT chart trajectory gets stuck around $SNR = 4$ dB. Then the mutual information after the iterative decoding can not become 1. Therefore, the BER performance can not become error free. From the comparison between Figs. 8 and 12, it is seen that the water fall exists at the region between $SNR = 4$ and 5 dB in the case where the outer code is the turbo code. On the other hand, in the case where the outer code is the convolutional code, it is seen that the water fall exists at the region between $SNR = 2$ and 3 dB. Therefore, the optimum type of outer code is not a turbo code but a convolutional code. We assumed that the input of the outer code is a Gaussian distribution. However, at the low channel values of outer decoder, there is some approximation error (Eq. (34)). Then, this analysis with the EXIT chart can not correspond to the BER simulation (Fig. 8) perfectly. From the comparison between Fig. 8 and Fig. 12, the amount of approximation error is very small (≤ 0.5 dB). Then the EXIT chart analysis is a valid analysis of STF turbo code.

6. Computational Complexity

In this section, we describe the computational complexity in the case where the outer code is convolutional or turbo code. The computational complexity depends mainly on the number of states and paths from each state. Therefore, we count the number of all paths from each state during decoding one OFDM frame. Consider that the number of states of the outer/inner code is St_o/St_i, the number of paths from each state in the case of the outer/inner code is Pa_o/Pa_i and that the number of iterations is N_{iter}. In the case that the outer code is a RSC or non-RC code and the inner code is a recursive or non-recursive space-frequency code, the computational complexity can be expressed as

$$C_c = \{(Pa_o \times St_o) \times N_c \times (N_s \times \log_2 |\mathcal{A}_X|) + (Pa_i \times St_i) \times N_c \times N_s\} \times N_{iter}. \quad (38)$$

We assign $Pa_o = 2, Pa_i = |\mathcal{A}_X|$ to Eq. (33), and it can be rewritten as

$$\begin{aligned} C_c &= (2St_oN_cN_s \log_2 |\mathcal{A}_X| + |\mathcal{A}_X|St_iN_cN_s) \times N_{iter} \\ &= N_cN_sN_{iter}(2St_o \log_2 |\mathcal{A}_X| + |\mathcal{A}_X|St_i). \end{aligned} \quad (39)$$

In the case that the outer code is a turbo code and the inner is a recursive or non-recursive space-frequency code, we define the number of iterations of the outer code (when the turbo code consists of two element encoders with St_o states) as N_{Tu}. The computational complexity can be expressed as

$$C_t = [\{2(Pa_o \times St_o) \times N_c \times (N_s \log_2 |\mathcal{A}_X|)\} \times N_{Tu} + (Pa_i \times St_i)N_cN_s] \times N_{iter}. \quad (40)$$

We assign $Pa_o = 2, Pa_i = |\mathcal{A}_X|$ to Eq. (35), therefore, it can be rewritten as

$$C_t = N_cN_sN_{iter}(4St_oN_{Tu} \log_2 |\mathcal{A}_X| + |\mathcal{A}_X|St_i). \quad (41)$$

Consider the concatenation between a 2-transmit QPSK 4state RSF code and a 7-5 non-RC code. Equation (34) is computed as

$$C_c = 32N_cN_sN_{iter}. \quad (42)$$

On the other hand, consider the concatenation between a 2-transmit QPSK 4state RSF code and a turbo code which consist two RSC codes. Equation (36) is computed as

$$C_t = N_cN_sN_{iter}(32N_{Tu} + 16). \quad (43)$$

In the case that we ignore the interleaver and deinterleaver function in the turbo (outer) code, the computational complexity of the concatenation between a RSF and a turbo codes is $(N_{Tu} + \frac{1}{2})$ times higher than the one between a RSF and non-RC codes.

7. Conclusion

This paper proposed and investigated a serial concatenated code over STF domain. The proposed STF turbo code can achieve high coding gain (interleaver gain) and diversity gain in STF domain due to the concatenation of different domain codes. We have expanded the EXIT chart analysis to the proposed STF turbo code. From the viewpoint of theoretical analysis utilizing the EXIT chart, the best structure of serial concatenation of different TF and SF codes can be designed with non-recursive outer (TF) encoder and recursive inner (SF) encoder. However, in case where the channel has spatial, temporal or frequency correlation, the STF turbo code in which the outer encoder is a turbo code has the best BER performance; whereas, this structure has a very high computational complexity. Additionally, in this paper, we have optimized the structure for the proposed STF turbo code. In general, however, since the performance of turbo code depends on each element encoder and the interleaver, we only considered the optimization of the structure for STF turbo code but not the optimization of element encoders and interleaver. Moreover, the future works are as follows:

- the optimization of each element encoder and interleaver for STF turbo code.
- The reduction of computational complexity on the iterative decoding process.
- The EXIT chart analysis in case where the channels have correlation.

Acknowledgments

The authors would like to extend my thank to assistant professor Hideki Ochiai for his advice and comments.

References

[1] G.F. Foschini, "Layered space-time architecture for wireless communication in a fading environment when using multiple antennas," Bell Labs. Tech. J., vol.1, no.2, pp.41–59, 1996.
[2] H. Sampath, P. Stoica, and A. Paulraj, "Generalized linear precoder and decoder design for MIMO channels using the weighted MMSE criterion," IEEE Trans. Commun., vol.49, no.12, pp.2198–2206, Dec. 2001.
[3] K. Ban, M. Katayama, T. Yamazato, and A. Ogawa, "Joint optimization of transmitter/receiver with multiple transmit/receive antennas in band-limited channels," IEICE Trans. Commun., vol.E83-B, no.8, pp.1697–1704, Aug. 2000.
[4] K. Miyashita, T. Nishimura, T. Ohgane, Y. Ogawa, Y. Takatori, and K. Cho, "High data-rate transmission with eigenbeam-space division multiplexing (E-SDM) in a MIMO channel," Proc. VTC2002-Fall, pp.1302–1306, Sept. 2002.
[5] V. Tarokh, N. Seshadri, and A.R. Calderbank, "Space-time codes for high data rate wireless communication: Performance criterion and code construction," IEEE Trans. Inf. Theory, vol.44, no.2, pp.744–765, March 1998.
[6] D. Tujkovic, "Recursive space-time trellis codes for turbo coded modulation," Proc. IEEE Global Telecomm. Conf., vol.2, pp.1010–1015, Nov. 2000.
[7] D. Tujkovic, M. Juntti, and M. Latva-aho, "Space-frequency-time turbo coded modulation," IEEE Commun. Lett., vol.5, no.12, pp.480–482, Dec. 2001.
[8] S. Zhou and G.B. Giannakis, "Space-time coding with maximum diversity gains over frequency-selective fading channels," IEEE Signal Process. Lett., vol.8, no.10, pp.269–272, Oct. 2001.
[9] H. Blölcskei and A.J. Paulraj, "Space-frequency coded broadband OFDM systems," Proc. Wireless Commun. Network Conf., pp.23–28, Sept. 2000.
[10] Z. Liu, Y. Xin, and G.B. Giannakis, "Space-time-frequency coded OFDM over frequency-selective fading channels," IEEE Trans. Signal Process., vol.50, no.10, pp.2465–2476, Oct. 2002.
[11] Z. Wang, S. Zhou, and G.B. Giannakis, "Joint coding-precoding with low-complexity turbo-decoding," IEEE Trans. Wirel. Commun., vol.3, no.3, pp.832–842, May 2004.
[12] S. Benedetto, D. Divsalar, G. Montorsi, and F. Pollara, "Serial concatenation of interleaved codes: Performance analysis, design, and iterative decoding," IEEE Trans. Inf. Theory, vol.44, no.3, pp.909–926, May 1998.
[13] S. Benedetto and G. Montorsi, "Iterative decoding of serially concatenated convolutional codes," Electron. Lett., vol.32. pp.1186–1188, June 1996.
[14] L.R. Bahl, J. Cocke, F. Jelinek, and J. Raviv, "Optimal decoding of linear codes for minimizing symbol error rate," IEEE Trans. Inf. Theory, vol.20, pp.284–287, July 1974.
[15] S. ten Brink, "Design of serially concatenated codes based on iterative decoding convergence," Proc. Second International Symposium on Turbo Codes and Related Topics, 2000.
[16] S. ten Brink, "Convergence behavior of iteratively decoded parallel concatenated codes," IEEE Trans. Commun., vol.49, no.10, pp.1727–1737, Oct. 2001.
[17] E. Biglieri, A. Nordio, and G. Taricco, "EXIT-chart analysis of iterative MIMO interfaces," Proc. ISITA, pp.1511–1516, Oct. 2004.
[18] F. Daneshgaran, M. Laddomada, and M. Mondin, "Interleaver design for serially concatenated convolutional codes: Theory and application," IEEE Trans. Inf. Theory, vol.50, no.6, pp.1177–1188, June 2004.
[19] S. Lin and D.J. Costello, Error Control Coding, Pearson Education, 2004.
[20] T.M. Cover and J.A. Thomas, Elements of Information Theory, Wiley, New York, 1991.

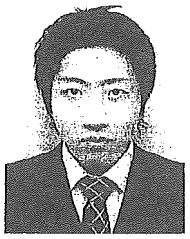

Kouji Ishii received the B.E., M.E., and Ph.D. degrees from Yokohama National University, Yokohama, Japan, in 2000, 2002, and 2005, respectively. He is now an Assistant of the Departmant of Reliability-based Information Systems Engineering at Kagawa University, Japan. He is a member of IEEE.

Ryuji Kohno received the Ph.D. degree from the University of Tokyo in 1984. Dr. Kohno is currently a Professor of the Division of Physics, Electrical and Computer Engineering, Yokohama National University. In his career he was a director of Advanced Telecommunications Laboratory of SONY CSL during 1998-2002 and currently a director of UWB Technology institute of National Institute of Information and Communications Technology (NICT). In his academic activities, he was elected as a member of the Board of Governors of IEEE Information Theory (IT) Society in 2000 and 2003. He has played a role of an editor of the IEEE Transactions on IT, Communications, and Intelligent Transport Systems (ITS). He is a vice-president of Engineering Sciences Society of IEICE and has been the Chairman of the IEICE Technical Committee on Spread Spectrum Technology, that on ITS, and that on Software Defined Radio (SDR). Prof. Kohno has contributed for organizing many international conferences, such as a chair-in honor of 2002 and 2003 International Conference of SDR (SDR'02 and SDR'03), a TPC co-chair of 2003 International Workshop on UWB Systems (IWUWBS'03), and a general co-chair of 2003 IEEE International Symposium on IT (ISIT'03), that of Joint UWBST & IWUWBS'04 and so on. He was awarded IEICE Greatest Contribution Award and NTT DoCoMo Mobile Science Award in 1999 and 2002, respectively.

IEICE TRANS. FUNDAMENTALS, VOL.E88–A, NO.10 OCTOBER 2005

PAPER Special Section on Information Theory and Its Applications

A Differential STBC Integrated with Trellis Coded Modulation

Susu JIANG[†a)], *Student Member*, Kentaro IKEMOTO[†*], *Member, and* Ryuji KOHNO[†], *Fellow*

SUMMARY We introduce a differential space-time block code (DSTBC) integrated with trellis coded modulation with two transmit antennas. Our scheme enables transmission of DSTBC encoded symbols as trellis metric rather than concatenating an outer code. Unlike conventional DSTBC, different transmit symbol phase rotations are used for each transmit antenna in order to obtain more options for trellis branch. The set partitioning for proposed codes is derived as well. The decoder computes decision statistic using Viterbi Algorithm with different number of states undergoing Rayleigh fading channels. This approach can provide full diversity gain as well as coding gain simultaneously remaining full transmit rate, which cannot be obtained by conventional DSTBC.

key words: *space-time code, differential space-time block code, symbol phase rotation, set partitioning*

1. Introduction

In wireless mobile communications, in order to reduce the system complexity of mobile users and enhance the broadband data access, it is important to develop a new system design that can achieve a higher frequency efficiency (transmit data rate per unit bandwidth) with a lower complexity. Alamouti proposed a space-time block code (STBC) [1] with a simple algorithm which exploits multiple antennas at the transmitter and obtain full diversity gain as we can obtain with multiple antennas at the receiver. STBC, however, does not provide any coding gain. On the other hand, space-time trellis code (STTC) introduced by Tarokh et al. can obtain the same diversity gain, and simultaneously can achieve coding gain [2]. Additionally, many papers have considered the concatenation of STBC and trellis codes [3]–[5] in order to achieve both diversity gain and coding gain. They evaluated the performance of concatenated STBC with trellis coded modulation in fading channels and found out that it usually performs better than Tarokh's STTC. Since then, many researches have been done on a large scale in order to reduce the complexity or to enhance the coding gain.

Most of the researches on space-time coding considers that the channel information can be estimated perfectly at the receiver, and is used for decoding. In case that the channel information is not available neither at the transmitter nor the receiver, the performance of space-time coding degrades a lot. For this reason, differential detection strategy for multiple transmit antennas has been investigated. For instance, B.M. Hochwald et al. considered the design of space-time modulation scheme that does not require channel estimation at the transmitter or receiver [6]. They proposed a general approach to differential modulation based on unitary group codes. B.L. Hughes presented a differential space-time modulation scheme [7] with a very similar way to that of [6], where the design for two transmit antennas is unique. Tarokh et al. introduced a different STBC based on orthogonal block designs (DSTBC) with two transmit antennas in [8], and with more than two transmit antennas in [9]. These differential schemes, however, do not obtain coding gain. Thus, it is very natural to exploit them with outer codes. The concatenated differential space-time code with trellis code is introduced in [10]–[13]. A DSTBC scheme with Turbo code concatenation introduced in [10] can achieve a very good coding gain in Rayleigh fading channels. L.H. Lamp et al. evaluated the concatenation scheme with various trellis coded modulation such as multilevel coding, bit-interleaved coded modulation, hybrid coded modulation and so on [12]. J.P.K. Chu et al. investigated the performance of convolutional code or Turbo codes concatenation in [13], and evaluated the effect of spatial cross-correlation between two fading channels. P.Tarasak et al. evaluated Ungerboeck outer code concatenation with perfect interleaving and provided a coding gain analysis [14]. Both the code concatenated with convolutional code and the code concatenated with Turbo code can achieve higher coding gain; however, the complexity at the receiver is also high. Moreover, due to the coding rate of outer code, these codes suffers from transmit rate loss (refer the upper part of Fig. 1).

In this paper, the existing differential STBC scheme (DSTBC) with two transmit antennas proposed by Tarokh is focused. A scheme that can achieve coding and diversity gain simultaneously, which cannot be obtained with conventional DSTBC scheme, is proposed. With conventional DSTBC scheme, the coding gain can only be obtained by concatenating outer codes such as Convolutional code, Turbo-code, LDPC and so on. We, inspired by Ungerboeck's trellis coded modulation scheme, proposed a trellis coded DSTBC scheme that can obtain coding gain without concatenating an outer-code (refer the lower part of Fig. 1). Our proposed scheme can simultaneously achieve diversity gain and coding gain. In more detail, we use phase rotation scheme to increase the number of the combinations of N_T transmit symbols, where N_T represents the number of

Manuscript received January 24, 2005.
Manuscript revised April 23, 2005.
Final manuscript received June 15, 2005.

[†]The authors are with the Graduate School of Engineering, Yokohama National University, Yokohama-shi, 240-8501 Japan.
[*]Presently, with Institute for Systems Research, University of Maryland, College Park, MD, USA.
a) E-mail: susu@kohnolab.dnj.ynu.ac.jp

DOI: 10.1093/ietfec/e88–a.10.2896

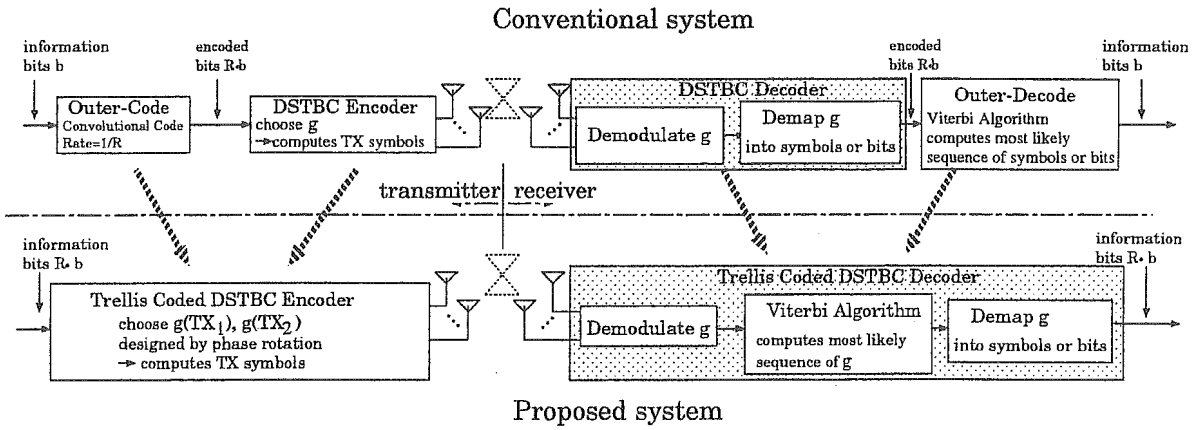

Fig. 1 System block diagram.

transmit antennas. These expanded combinations then are encoded and act as trellis metrics in order to obtain coding gain. We call it Coded DSTBC scheme. Moreover, in order to design codes in a systematic way, we also proposed a set partitioning applicable to DSTBC scheme, and according to this set partitioning, one can easily design codes matching an expected coding gain and a transmit rate. Due to the coding rate of outer-codes, the transmit rate decreases when we use the conventional DSTBC scheme. However, our proposed code maintains the full transmit rate while obtaining coding gain. Note that full-rate transmission satisfies b bits/s/Hz transmission, where b is the information bits and b=$\log_2 M$ with MPSK modulation. In addition, with conventional DSTBC scheme, two computational processes have to be used at the transmitter, outer encoder and DSTBC encoder process. With our proposed scheme, only DSTBC encoder is needed in addition to a phase rotation structure. The receiver side includes DSTBC decoder demodulating received symbols and a Viterbi Algorithm to make a most likely sequence decision according to the received symbols. The details are shown in Sect. 3.

The rest of this paper is structured as follows. Section 2 describes the system model and provides pairwise error probability for our scheme. The detailed coded DSTBC design is introduced in Sect. 3, and the numerical coding gain analysis and simulation results are shown in Sect. 4. Finally, we draw a short conclusion in Sect. 5.

2. Preliminaries

The system model of differential space-time block code and its pairwise error probability are derived in this section, respectively.

2.1 System Description

Assuming a wireless channel in which data are sent from $N_T = 2$ transmit antennas and received by N_R receive antennas undergoing a Rayleigh flat fading channels, where the channel path gains are constant during a frame and vary independently from one frame to another (quasi-static flat fading). The channel information is not available neither at the transmitter nor at the receiver, therefore, the differential detection is used. We restrict the constellation point c_i^t at i-th antenna and t-th time slot (i=1,$\cdots$,N_T; t=0,1,$\cdots$) to MPSK (M=2^b) for the information bits b=1,2,$\cdots$, and c_i follows,

$$c_i = \frac{\exp(2\pi k j/M)}{\sqrt{N_t}} \quad \Big| \quad k = 0, 1, \cdots, M-1, \tag{1}$$

where $j^2 = -1$. DSTBC uses a unique encoder algorithm exploiting an encoder coefficient vector $\mathcal{G}$=($\mathcal{G}_1, \mathcal{G}_2$). When there are two transmit antennas, for any combination of constellation points c_1 and c_2, $\mathcal{G}$ is defined by,

$$\begin{aligned} \mathcal{G} &= (\mathcal{G}_1, \mathcal{G}_2) \\ &= (c_1^{ini^*} c_1 + c_2^{ini^*} c_2, -c_2^{ini} c_1 + c_1^{ini} c_2), \end{aligned} \tag{2}$$

where c_i^{ini} (i=1,2) indicates initial value for MPSK of encoder algorithm. Since MPSK constellation points always contains the point $1/\sqrt{2}$, the initial values (c_1^{ini}, c_2^{ini})=($1/\sqrt{2}$, $1/\sqrt{2}$) are used. Therefore, considering all the combinations of c_1 and c_2, there are M^2 different $\mathcal{G}$ for MPSK modulation, which results in full-rate transmission b bits/s/Hz. In other words, each combination of c_1 and c_2 has a corresponding vector $\mathcal{G}$. In DSTBC encoder algorithm, this coefficient vector $\mathcal{G}$ is chosen according to the combination of c_1 and c_2. DSTBC considers four time slots as one set to encode and decode, here, let us assume four time slots $2t$, $2t+1$, $2t+2$, $2t+3$. Assuming at time slot $2t$ and $2t+1$, two b information bits are mapped into c_1^{2t} and c_2^{2t}, and encoded into transmit symbols s_1^{2t} and s_2^{2t}, where s_i^t indicates the transmit symbol at i-th antenna and t-th time slot. Define the orthogonal symbol transmission matrix by,

$$\mathbf{S}_{2t,2t+1} = \begin{pmatrix} s_1^{2t} & s_2^{2t} \\ -s_2^{2t*} & s_1^{2t*} \end{pmatrix}, \tag{3}$$

where the row indicates the transmit time slot 2t and 2t+1, and $\mathbf{S}_{2t,2t+1}$ represents the symbol set transmitted at time slot 2t and 2t+1 from each antenna. At the next two time slots, the transmitter maps the next two b bits into c_1^{2t+2} and c_2^{2t+2}

for each antenna. According to these c_1^{2t+2} and c_2^{2t+2}, the corresponded $\mathcal{G}$ is chosen following Eq. (2) in order to encode these two symbols to be transmitted from each antenna. The next two symbols, therefore, are given by,

$$\begin{aligned}(s_1^{2t+2}, s_2^{2t+2}) &= \mathcal{G} \cdot \mathbf{S_{2t,2t+1}} \\ &= (\mathcal{G}_1 s_1^{2t} - \mathcal{G}_2 s_2^{2t*}, \mathcal{G}_1 s_2^{2t} + \mathcal{G}_2 s_1^{2t*}).\end{aligned} \tag{4}$$

In addition, the transmit symbol set $\mathbf{S_{2t+2,2t+3}}$ at the next two time slots $2t+2$ and $2t+3$ is defined by,

$$\mathbf{S_{2t+2,2t+3}} = \begin{pmatrix} s_1^{2t+2} & s_2^{2t+2} \\ -(s_2^{2t+2})^* & (s_1^{2t+2})^* \end{pmatrix}. \tag{5}$$

The received signal at time slot t is given by,

$$r_t^j = \sum_{i=1}^{N_T} \alpha_{i,j} s_i^t + n_{i,j}^t. \tag{6}$$

The coefficient $\alpha_{i,j}$ is the path gain from transmit antenna i to receive antenna j, and $n_{i,j}^t$ is the noise. With two transmit antennas, the receiver then computes two factors as follows,

$$\begin{aligned}\mathcal{R}_1^j &= r_{2t+2}^j r_{2t}^{j*} + r_{2t+3}^{j*} r_{2t+1}^j \\ &= (|\alpha_{1,j}|^2 + |\alpha_{2,j}|^2)(s_1^{2t*} s_1^{2t+2} + s_2^{2t*} s_2^{2t+2}) + \mathcal{N}_1^j, \\ \mathcal{R}_2^j &= r_{2t+2}^j r_{2t+1}^{j*} - r_{2t+3}^{j*} r_{2t}^j \\ &= (|\alpha_{1,j}|^2 + |\alpha_{2,j}|^2)(-s_2^{2t} s_1^{2t+2} + s_1^{2t} s_2^{2t+2}) + \mathcal{N}_2^j.\end{aligned} \tag{7}$$

Note that for the sake of simplicity, $\mathcal{N}_i^j$ $(i=1,2)$ indicates all the terms that include the Gaussian noise factor $n_{i,j}^t$ at j-th receive antenna. Calculating $\mathcal{G}_1$ and $\mathcal{G}_2$ from Eq. (4), we obtain,

$$\begin{aligned}\mathcal{R}_1^j &= (|\alpha_{1,j}|^2 + |\alpha_{2,j}|^2)\mathcal{G}_1 + \mathcal{N}_1^j, \\ \mathcal{R}_2^j &= (|\alpha_{1,j}|^2 + |\alpha_{2,j}|^2)\mathcal{G}_2 + \mathcal{N}_2^j.\end{aligned} \tag{8}$$

Therefore, when there are N_R receive antennas, the receiver makes a decision by looking for the closest vector $\mathcal{G}=(\mathcal{G}_1, \mathcal{G}_2)$ to $(\sum_{j=1}^{N_R} \mathcal{R}_1^j, \sum_{j=1}^{N_R} \mathcal{R}_2^j)$. Once the vector $\mathcal{G}$ is estimated, the symbols c_i can be demapped, and the information bits are recovered.

Four properties are also provided in [8]. We, here, introduce three of them in order to make a comparison to ours in next section.

- Property A: It has 2^{2b} elements corresponding to the pairs (c_1, c_2) of constellation symbols.
- Property B: All elements of $\mathcal{G}$ have unit length.
- Property C: The minimum distance between any two distinct elements of $\mathcal{G}$ is equal to the minimum distance of MPSK constellation points.

2.2 Pairwise Error Probability

A very simple pairwise error probability (PEP) is given in [14] for MPSK. Let us consider the receiver estimates erroneously in favor of a sequence $\tilde{r}=(\tilde{r}_1^t, \tilde{r}_2^t) \in \mathcal{G}$ assuming that $r=(r_1^t, r_2^t)$ were transmitted at t-th time slot. The probability of deciding $\tilde{r}$ while transmitting r is given by $P(\tilde{r} \to r)=P(\mu(\mathcal{R}, \tilde{r}) \geq \mu(\mathcal{R}, r))$. PEP then can be obtained by Eq. (9) applying Chernoff bound.

$$\begin{aligned}&P(\tilde{r} \to r) \\ &\leq \prod_{j=1}^{N_R} \prod_{l} E\Big[\exp(\delta \Re[(|\mathcal{R}_1^j - r_1|^2 - |\mathcal{R}_1^j - \tilde{r}_1|^2) \\ &\quad + (|\mathcal{R}_2^j - r_2|^2 - |\mathcal{R}_2^j - \tilde{r}_2|^2)])\Big] \\ &= \prod_{j=1}^{N_R} \prod_{l} E\Big[\exp(2\delta \Re[\mathcal{R}_1^j(\tilde{r}_1^* - r_1^*) + \mathcal{R}_2^j(\tilde{r}_2^* - r_2^*)])\Big].\end{aligned} \tag{9}$$

Note that l is the set in which $(\tilde{r}_l \neq r_l)$ or $(\tilde{r}_l \neq r_l)$ and δ is a Chernoff parameter to be optimized. Assigning Eq. (7) into Eq. (9), optimizing by $(\partial P/\partial \delta)$ [14], the PEP is finally given by,

$$\begin{aligned}P(\tilde{r} \to r) \leq \prod_{j=1}^{N_R} \prod_{l} \Big[&\exp\left(-\frac{E_s}{16N_0}(|\alpha_{1,j}|^2 + |\alpha_{2,j}|^2\right) \\ &\cdot(|\tilde{r}_1 - r_1|^2 + |\tilde{r}_2 - r_2|^2)\Big].\end{aligned} \tag{10}$$

In case that the sequence undergoes Rayleigh flat fading channel where the path gain is constant over a frame length and vary independently from one frame to another frame, Eq. (10) can be averaged considering a high SNR approximation by,

$$\begin{aligned}P(\tilde{r} \to r) &\leq \prod_{j=1}^{N_R} \left(\frac{E_s}{16N_0} d_{free}^2(\tilde{r}, r)\right)^{-2} \\ &= \left(\frac{E_s}{16N_0} d_{free}^2(\tilde{r}, r)\right)^{-2N_R},\end{aligned} \tag{11}$$

where $d_{free}^2(\tilde{r}, r)=\sum_l(|\tilde{r}_1 - r_1|^2+|\tilde{r}_2 - r_2|^2)$.

According to Eq. (11), therefore, in order to obtain the coding gain, one needs to find a good sequence that maximize $d_{free}^2(\tilde{r}, r)$. We propose a code design in next section so as to obtain large $d_{free}^2(\tilde{r}, r)$.

3. Proposed Coded DSTBC

We provide our proposed coded DSTBC scheme in this section. The encoder and the decoder are described respectively.

3.1 Encoding for MPSK

As described in previous section, DSTBC encoder maps symbols into a vector $\mathcal{G}$ and calculates two transmit symbols sent from two antennas. The decoder computes the closest

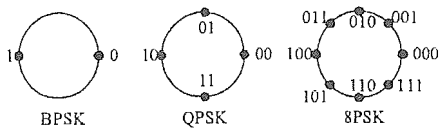

Fig. 2 Constellation for MPSK.

vector sequence $\tilde{r}\in\mathcal{G}$ to the receive sequence r. Therefore, the distance between any two distinct elements of $\mathcal{G}$ dominates the system performance. In order to achieve coding gain, we now propose a scheme to assign each vector of $\mathcal{G}$ to trellis branch. For the sake of simplicity, let us consider a two-state trellis code. There are M^2 different elements of $\mathcal{G}$ in conventional DSTBC scheme, therefore, to avoid transmission rate loss, we have to assign all M^2 vectors $\mathcal{G}$ to the branches diverging from one state, assuming it is state 0. As for state 1, however, if we assign the same M^2 vectors $\mathcal{G}$ to the branches diverging from state 1, obviously there exists branches having the same vectors as those diverging from state 0. This results in a catastrophic code. Consequently, we propose a scheme to increase the number of vector $\mathcal{G}$ so as to assign them to branches diverging from another state.

We use different symbol phase rotation for each transmit antenna. The constellation for MPSK is shown in Fig. 2. Assume that the mapped symbols c_i at one antenna are from this constellation and denoted by Eq. (1). The symbols at another antenna are all rotated by $\theta = \frac{\pi}{M}$, thus can be denoted by $c_i e^{j\frac{\pi}{M}}$. The modulation scheme for this antenna, therefore, is still MPSK modulation. To obtain vector $\mathcal{G}$, the initial symbols have to be chosen. Let us denote $\mathcal{G}(TX_i)$ $(i = 1, 2)$ to be the coefficient having symbol phase rotation $e^{j\frac{\pi}{M}}$ at i-th antenna, TX_i indicates i-th transmit anntena with transmitted symbols having phase rotation of θ. In case that antenna 1 always contains symbols $c_i e^{j\frac{\pi}{M}}$, the initial value can be defined by $c_1^{ini}=(1/\sqrt{2})e^{j\frac{\pi}{M}}$. The symbols at antenna 2 are always from the original constellation, therefore, the initial value can be defined by $c_2^{ini}=(1/\sqrt{2})$. Using these initial values, the vector $\mathcal{G}(TX_1)$ can be calculated following Eq. (2). Same as $\mathcal{G}(TX_1)$, $\mathcal{G}(TX_2)$ then can be obtained by using the initial value $c_1^{ini}=(1/\sqrt{2})$ and $c_2^{ini}=(1/\sqrt{2})e^{j\frac{\pi}{M}}$. $\mathcal{G}(TX_1)$ and $\mathcal{G}(TX_2)$ are finally given by,

$$\begin{aligned}\mathcal{G}(TX_1) &= (\mathcal{G}_{1_{TX_1}}, \mathcal{G}_{2_{TX_1}}) \\ &= \left(\frac{1}{\sqrt{2}}e^{-j\theta}c_1 + \frac{1}{\sqrt{2}}c_2, -\frac{1}{\sqrt{2}}c_1 + \frac{1}{\sqrt{2}}e^{j\theta}c_2\right), \\ \mathcal{G}(TX_2) &= (\mathcal{G}_{1_{TX_2}}, \mathcal{G}_{2_{TX_2}}) \\ &= \left(\frac{1}{\sqrt{2}}c_1 + \frac{1}{\sqrt{2}}e^{-j\theta}c_2, -\frac{1}{\sqrt{2}}e^{j\theta}c_1 + \frac{1}{\sqrt{2}}c_2\right),\end{aligned} \tag{12}$$

where $\theta=\frac{\pi}{M}$. For instance, with BPSK, the initial value for $\mathcal{G}(TX_1)$ becomes $(c_1^{ini}, c_2^{ini})=(\frac{1}{\sqrt{2}}j, \frac{1}{\sqrt{2}})$, and for $\mathcal{G}(TX_2)$ becomes $(c_1^{ini}, c_2^{ini})=(\frac{1}{\sqrt{2}}, \frac{1}{\sqrt{2}}j)$. $\mathcal{G}(TX_1)$ and $\mathcal{G}(TX_2)$, therefore, are given by $\mathcal{G}(TX_1)=(-\frac{1}{\sqrt{2}}jc_1+\frac{1}{\sqrt{2}}c_2, -\frac{1}{\sqrt{2}}c_1+\frac{1}{\sqrt{2}}jc_2)$, $\mathcal{G}(TX_2)=(\frac{1}{\sqrt{2}}c_1-\frac{1}{\sqrt{2}}jc_2, -\frac{1}{\sqrt{2}}jc_1+\frac{1}{\sqrt{2}}c_2)$. Considering all the

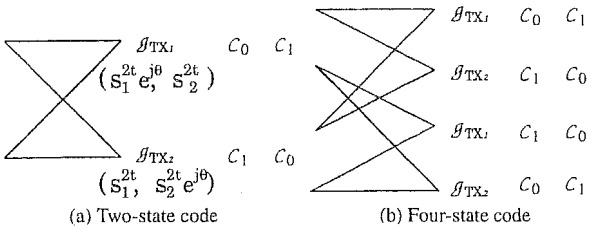

(a) Two-state code (b) Four-state code

Fig. 3 Trellis diagram for two- and four-state code.

combinations of c_1 and c_2, both $\mathcal{G}(TX_1)$ and $\mathcal{G}(TX_2)$ consist of M^2 elements. After choosing an appropriate $\mathcal{G}(TX_1)$ or $\mathcal{G}(TX_2)$, the encoder additionally computes the transmit symbols as shown in Eq. (4) and Eq. (5), and transmit them from both antennas. The decoder then calculates a function to obtain $\mathcal{G}(TX_1)$ or $\mathcal{G}(TX_2)$ in order to demap the transmit symbols thus the information bits.

The total system block diagram is shown in Fig. 1. Briefly, at the transmitter side, conventional code first encodes b information bits with outer-code, and then obtains $R \cdot b$ encoded bits when the coding rate of convolutional code is $\frac{1}{R}$. Finally, these $R \cdot b$ bits are encoded by DSTBC encoder again from bits to $R \cdot b/\log_2 M$ symbols (note that MPSK modulation is used) and transmitted from antennas. Therefore, only b information bits can be transmitted. On the other hand, the proposed code can once input $R \cdot b$ information bits into DSTBC encoder, and according to these $R \cdot b$ information bits, it generates two groups of coefficients $\mathcal{G}(TX_1)$ and $\mathcal{G}(TX_2)$ in order to represent all the information bits; while with conventional scheme, there is only one group of $\mathcal{G}$. After generating $\mathcal{G}(TX_1)$ and $\mathcal{G}(TX_2)$, we assign them to trellis as shown in Fig. 3. Finally, $R \cdot b/\log_2 M$ transmit symbols are achieved by Eq. (4), and transmitted from antennas. Therefore, our proposed code can transmit $R \cdot b$ information bits once. In conclusion, at the transmitter, conventional outer-code encodes information bits; however, proposed coded DSTBC encodes the coefficient $\mathcal{G}(TX_1)$ and $\mathcal{G}(TX_2)$.

Before we assign $\mathcal{G}(TX_1)$ and $\mathcal{G}(TX_2)$ to different trellis state, however, we need to prove that these two groups of $\mathcal{G}$ have all distinct elements. Obviously, all elements in the same $\mathcal{G}(TX_i)$ are distinct. Now we need to consider the elements in different group of $\mathcal{G}$. Let us first consider $\mathcal{G}(TX_2)=(\mathcal{G}_{1_{TX_2}}, \mathcal{G}_{2_{TX_2}})$ shown in Eq. (12). c_1 is a symbol from the original constellation and denoted by $c_1=\frac{1}{\sqrt{2}}e^{j\beta}$, where $\beta = \frac{2k\pi}{M}$; while c_2 is from phase rotated constellation and denoted by $c_2=\frac{1}{\sqrt{2}}e^{j\beta'+\theta'}$, where $\theta'=\frac{2k'\pi}{M} + \frac{\pi}{M}$. $\mathcal{G}_{1_{TX_2}}$ and $\mathcal{G}_{2_{TX_2}}$, therefore, finally can be obtained by,

$$\begin{aligned}\mathcal{G}_{1_{TX_2}} &= \frac{1}{2}(e^{j\beta} + e^{j(\beta'+\theta'-\theta)}) \\ &= \frac{1}{2}(e^{j\beta} + e^{j(\beta'+\beta'')}), \\ \mathcal{G}_{2_{TX_2}} &= -\frac{1}{2}(e^{j(\beta+\theta)} + e^{j(\beta'+\theta')}).\end{aligned} \tag{13}$$

Note that θ'-θ is the phase rotation belonging to β. Obvi-

ously, $\mathcal{G}_{1_{TX_2}}$ and $\mathcal{G}_{2_{TX_2}}$ have phase difference of $\theta = \frac{\pi}{M}$. Using the same criteria, $\mathcal{G}_{1_{TX_1}}$ and $\mathcal{G}_{2_{TX_1}}$ can be calculated, and $\mathcal{G}_{1_{TX_1}}$ has symbol phase belonging to θ that is the same as that of $\mathcal{G}_{2_{TX_2}}$, and $\mathcal{G}_{2_{TX_1}}$ has symbol phase belonging to β that is the same as that of $\mathcal{G}_{1_{TX_2}}$. Clearly, due to the phase difference, $\mathcal{G}_{1_{TX_1}}$ is different from $\mathcal{G}_{1_{TX_2}}$, and $\mathcal{G}_{2_{TX_1}}$ is different from $\mathcal{G}_{1_{TX_2}}$ in Eq. (12). Therefore, for MPSK, the elements in $\mathcal{G}(TX_1)$ and $\mathcal{G}(TX_2)$ are all different from each other.

In order to obtain better coding gain, we need to organize the distance between any two elements in $\mathcal{G}(TX_1)$ or $\mathcal{G}(TX_2)$, thus d^2_{free}. Set partitioning is designed as shown in Fig. 4, Fig. 5, Fig. 6 and Fig. 7. C_i (i=0,1) indicates the stage of set partitioning. The indications at each branch leaf represent $2\log_2 M$ information bits transmitted from antenna 1 and 2. In more detail, first $\log_2 M$ bits are mapped into c_1 and next $\log_2 M$ bits are mapped into c_2 to be used to obtain an element of $\mathcal{G}$, Eq. (12). These set partitionings are therefore designed so that the distance between any two elements of $\mathcal{G}$ is the maximum at each corresponding stage. Note that these set partitionings can be used for both $\mathcal{G}(TX_1)$ and $\mathcal{G}(TX_2)$. Therefore, c_1 or c_2 is phase rotated according to which group of $\mathcal{G}$ is used. While we design the set partitioning for the proposed DSTBC, we first tried to design a stage having much larger distance between any two elements in $\mathcal{G}(TX_1)$ or $\mathcal{G}(TX_2)$ (Fig. 4, Fig. 5 and Fig. 6). For BPSK, the last stage has the largest distance $d^2_{free} = 4$ and for 8PSK is $d^2_{free} = 1$. For QPSK, the largest distance we can design is $d^2_{free} = 4$, however, with two-state code, the code designed according to this set partitioning performs much worse than the codes designed following the set partitioning Fig. 7, which are constructed according to the information bits so as to obtain larger hamming distance. The detail is analyzed in Sect. 4.

Referring to these set partitionings, we provide three properties compared to Tarokh's.

- Property A: It has $2 \cdot 2^{2b}$ elements corresponding to the pairs $(c_1, c_2 e^{j\theta})$ and $(c_1 e^{j\theta}, c_2)$ of constellation symbols.
- Property B: All elements of $\mathcal{G}$ have unit length.
- Property C: The minimum distance between any two distinct elements of $\mathcal{G}$ is equal to the minimum distance of MPSK constellation points.

We next assign two groups of $\mathcal{G}$, $\mathcal{G}(TX_1)$ and $\mathcal{G}(TX_2)$, to trellis branches as shown in Fig. 3. With two-state code, half elements C_0 of $\mathcal{G}(TX_1)$ are assigned to the state transition from 0 to 0, and the rest half C_1 are assigned to the state transition from 0 to 1. Likewise, half elements C_0 of $\mathcal{G}(TX_2)$ are assigned to the state transition from 1 to 1, and the rest half C_1 are assigned to the state transition from 1 to 0. According to the set partitioning, it is obviously that there exists several parallel paths for each state transition. Therefore, the distance between these parallel paths dominates the system performance. We call these parallel paths *length-1 error event*, and the distance between them *intra-distance*. More detail, according to the symbol set partitioning Fig. 4, Fig. 5 and Fig. 6, at the stage C_0 and C_1, the intra-distance is 4, 2 and 1 respectively for BPSK, QPSK and 8PSK. Additionally, the distance considering more than length-1 error event has to be larger than the intra-distance so as to achieve the maximum coding gain. We call this *inter-distance*. We describe the detail of inter-distance and total coding gain calculation in Sect. 4.1.

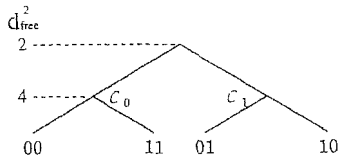

Fig. 4 Set partitioning for BPSK according symbols.

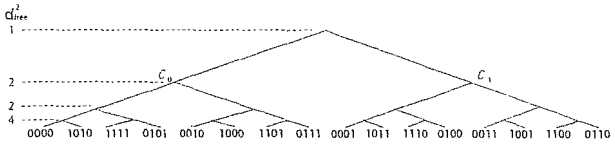

Fig. 5 Set partitioning for QPSK according to symbols.

3.2 Decoding for MPSK

We use different symbol phase rotation at different antenna

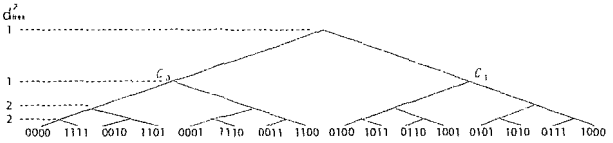

Fig. 7 Set partitioning for QPSK according to bits.

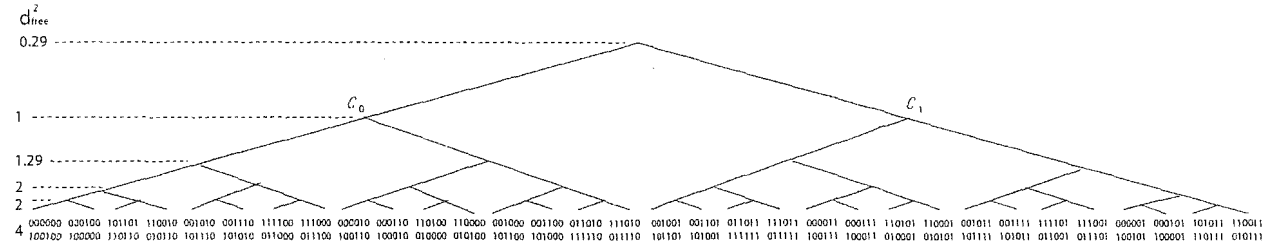

Fig. 6 Set partitioning for 8PSK according to symbols.

in order to encode the information bits according to proposed DSTBC encoding algorithm Eq. (12) as described in Sect. 3.1. Tarokh's DSTBC uses the coefficient $\mathcal{G}$ since according to the decoder algorithm, the receiver can obtain the same coefficient $\mathcal{G}$ so as to demap the symbols. We also utilize Tarokh's decoder algorithm as shown in Eq. (7). Since the proposed $\mathcal{G}(TX_1)$ and $\mathcal{G}(TX_2)$ include phase rotated symbols, according to Eq. (4), we can confirm that the transmit symbols in Eq. (5) from each antenna also include the phase difference of θ. The receiver then computes,

$$\begin{aligned}\mathcal{R}_1^j &= r_{2t+2}^j r_{2t}^{j*} + r_{2t+3}^{j*} r_{2t+1}^j \\ &= \begin{cases} (|\alpha_{1,j}|^2 + |\alpha_{2,j}|^2)\mathcal{G}_{1_{TX_1}} + \mathcal{N}_1^j \\ \quad or \\ (|\alpha_{1,j}|^2 + |\alpha_{2,j}|^2)\mathcal{G}_{1_{TX_2}} + \mathcal{N}_1^j, \end{cases} \end{aligned} \tag{14}$$

$$\begin{aligned}\mathcal{R}_2^j &= r_{2t+2}^j r_{2t+1}^{j*} - r_{2t+3}^{j*} r_{2t}^j \\ &= \begin{cases} (|\alpha_{1,j}|^2 + |\alpha_{2,j}|^2)\mathcal{G}_{2_{TX_1}} + \mathcal{N}_2^j \\ \quad or \\ (|\alpha_{1,j}|^2 + |\alpha_{2,j}|^2)\mathcal{G}_{2_{TX_2}} + \mathcal{N}_2^j. \end{cases} \end{aligned} \tag{15}$$

These two received symbols $\mathcal{R}_1^j$ and $\mathcal{R}_2^j$ are then used as trellis metrics and input to trellis. The Viterbi algorithm is used for decoding following the trellis diagram shown in Fig. 3 in order to estimate the most likely sequence of $\mathcal{G}(\mathcal{G}(TX_1)$ or $\mathcal{G}(TX_2))$ to the receive sequence $(\sum_{j=1}^{N_R}\mathcal{R}_1, \sum_{j=1}^{N_R}\mathcal{R}_2)$.

In order to make a comparison with conventional code, Fig. 1 shows the difference. At receiver side, conventional code first decodes the received symbols using DSTBC decoder and obtains the coefficient $\mathcal{G}$. According to $\mathcal{G}$, the DSTBC decoder also demaps $\mathcal{G}$ in order to obtain $R \cdot b/\log_2 M$ symbols. These $R{\cdot}b/\log_2 M$ symbols corresponds to $R \cdot b/\log_2 M$ symbols at transmitter side. And these $R \cdot b/\log_2 M$ symbols are input to the rate $\frac{1}{R}$ decoder in order to achieve a most likely sequence of b bits using Viterbi Algorithm. On the other hand, the proposed code decodes the received symbols using the same DSTBC decoder first, and obtain the coefficient $\mathcal{G}(TX_1)$ or $\mathcal{G}(TX_2)$. At next step, proposed code does not demap $R{\cdot}b/\log_2 M$ symbols as conventional code does, it directly inputs the coefficient $\mathcal{G}(TX_1)$ and $\mathcal{G}(TX_2)$ into trellis, and choose a most likely $\mathcal{G}(TX_1)$ and $\mathcal{G}(TX_2)$ sequence using Viterbi Algorithm. Once we get the estimated $\mathcal{G}(TX_1)$ and $\mathcal{G}(TX_2)$ sequence, we demap this sequence into $R{\cdot}b/\log_2 M$ symbols and the $R{\cdot}b$ information bits can also be recovered. In conclusion, at the receiver, conventional outer-decoder decodes symbols; however, proposed decoder decodes the coefficient $\mathcal{G}(TX_1)$ and $\mathcal{G}(TX_2)$.

4. Numerical Evaluation

This section describes the coding gain analysis and computer simulation results respectively.

4.1 Free Distance

As described above, the proposed set partitioning for QPSK two-state code considers the information bits so as to have large hamming distance between each other (Fig. 7). Another set partitioning we can design is the one considering d_{free}^2 so as to have large distance between any two distinct coefficient vector $\mathcal{G}$ (Fig. 5). By the computer search, however, we found out that the code utilizing the set partitionging considering bit hamming distance has better performance than that of the one utilizing the set partitioning considering symbol distance with two-state code. We first consider the symbol set partitioning for BPSK, QPSK and 8PSK (Fig. 4, Fig. 5, Fig. 6). According to the proposed set partitioning, the intra-distances are 4, 2, 1 for BPSK, QPSK and 8PSK respectively. The intra-distance is length-1 error event, and dominates the system performance.

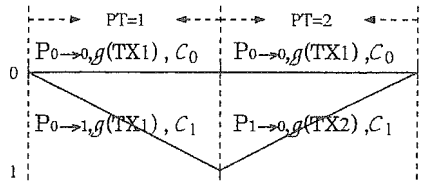

Fig. 8 Path transition for length-2 error events.

We next need to consider the inter-distance. In order to achieve maximum coding gain, the inter-distance has to be larger than the intra-distance. Assuming length-2 error event path transition, as shown in Fig. 8, $(P_{x\to y}, \mathcal{G}(TX_v), C_z)$ indicates the branches, *i.e.*, a set of the coefficient vector from $\mathcal{G}_{TX_v}$ $(v = 1, 2)$ corresponding to the set partitioning stage C_z $(z = 0, 1)$, for the path from state x to state y. For instance, let us consider the path diverging from state 0 and remerging into state 0 after two path transitions. Note again that the distance between any two branches $P_{x\to y}$ at stage C_z $(z = 0, 1)$ represents the intra-distance. As can be seen, at the first path transition $PT = 1$, the path $P_{0\to 0}$ and $P_{0\to 1}$ use different set C_0 and C_1 from the same encoder coefficient $\mathcal{G}(TX_1)$. According to the set partitioning, the intra-distance is larger than the distance between C_0 and C_1. We next consider the path transitions $P_{0\to 0}$ and $P_{1\to 0}$ at the second path transition $PT = 2$. These are from different encoder coefficient $\mathcal{G}(TX_1)$ and $\mathcal{G}(TX_2)$. In order to calculate the minimum distance among all elements of these two coefficients, we refer Eq. (12) to obtain the mean squared distance $d_{free}^{2'}$. Assuming c_1 and c_2 in $\mathcal{G}(TX_1)$ are different from those in $\mathcal{G}(TX_2)$, and the phase difference between c_1 and c_2 is δ_1 for $\mathcal{G}(TX_1)$ and δ_2 for $\mathcal{G}(TX_2)$, the minimum symbol distance is then given by,

$$\begin{aligned} d_{free}^{2'} &= |\mathcal{G}_{1_{TX_1}} - \mathcal{G}_{1_{TX_2}}|^2 + |\mathcal{G}_{2_{TX_1}} - \mathcal{G}_{2_{TX_2}}|^2 \\ &= \frac{1}{2}|1 - e^{-j\theta}|^2[|(c_1 - c_2)|^2 + |(c_1' + c_2')|^2] \\ &= (1 - \cos\theta)(|c_1 - c_2|^2 + |c_1' + c_2'|^2) \\ &= (1 - \cos\theta)[2 + (\cos\delta_2 - \cos\delta_1)]. \end{aligned} \tag{16}$$

According to Eq. (16), the minimum distance of $d_{free}^{2'}$ can be obtained when $\cos\delta_2 - \cos\delta_1 = 0$. Therefore, $\min d_{free}^{2'}$ for different phase rotation θ is given by,

$$\min d_{free}^{2'} = 2(1 - \cos\theta)$$

$$= \begin{cases} 2 & (\theta = \frac{\pi}{2}, BPSK) \\ 0.5858 & (\theta = \frac{\pi}{4}, QPSK) \\ 0.1522 & (\theta = \frac{\pi}{8}, 8PSK) \end{cases} \quad (17)$$

As described above, the inter-distance of length-2 error event for proposed MPSK differential DSTBC can be given by adding the distance between $P_{0\to 0}$ and $P_{0\to 1}$ to the distance between $P_{0\to 0}$ and $P_{1\to 0}$. Therefore, the inter-distance is $2 + 2 = 4$ for BPSK, $1 + 0.5858 = 1.5858$ for QPSK, $0.2929 + 0.1522 = 0.4451$ for 8PSK. Using the same evaluation, it is easy to show that the minimum value of the inter-distance when path transition is more than length-2 is greater than that of length-1 and increases as the length increases. For BPSK, the inter-distance for length-2 error event is obviously the same as the intra-distance, therefore, the optimum coding gain for BPSK is 4, and it can be designed with two-state code. QPSK, however, cannot achieve the maximum coding gain with two-state code since the inter-distance is smaller than the intra-distance. Therefore, the number of states needs to be increased. Considering length-3 error event, according to the description above, the inter-distance can be obtained as $1 + 0.5858 + 1 = 2.5858$, which is larger than the intra-distance. Four-state code, therefore, can maximize the coding gain for QPSK. The code for 8PSK needs much more number of states in order to achieve the maximum coding gain. Length-5 error event has $0.2929 + 0.1522 + 0.2929 + 0.1522 + 0.1522 = 1.0424$ inter-distance that is larger than the intra-distance. Sixteen-state code, therefore, can be considered to be the optimum code. However, we found out that with more than eight-state code for 8PSK, since d^2_{free} is very small, the performance does not significantly improve as we expected. We summarize the coding gain analysis in Table 1. Note that with Tarokh's DSTBC scheme, the minimum distance between any two elements of $\mathcal{G}$ is 2 for BPSK, 1 for QPSK, 0.2929 for 8PSK respectively. It can be seen that even with two-state code, our proposed codes can achieve larger coding gain than that of Tarokh's.

In terms of the bit set partitioning shown in Fig. 7, the intra-distance is 1, and the inter-distance can be easily obtained to be $1 + 0.5858 = 1.5858$, which is the same as the one using the symbol set partitioning Fig. 5. The code designed following Fig. 7, however, performs better. One of the possible reasons that we can think is that the distance of error events with length more than 2 is larger than if we use the symbol set partitioning.

Table 1 Coding gain comparison with Fig. 3 constructure.

	Tarokh d^2_{free}	Intra-distance of Proposed Codes	Inter-distance of Proposed Codes		d^2_{free}
			No. of states		
BPSK	2	4	2	4	4
			4	6	4
QPSK	1	2	2	1.5858	1.5858
			4	2.5858	2
8PSK	0.2929	1	2	0.4451	0.4451
			4	0.7380	0.7380
			8	0.8902	0.8902
			16	1.0424	1

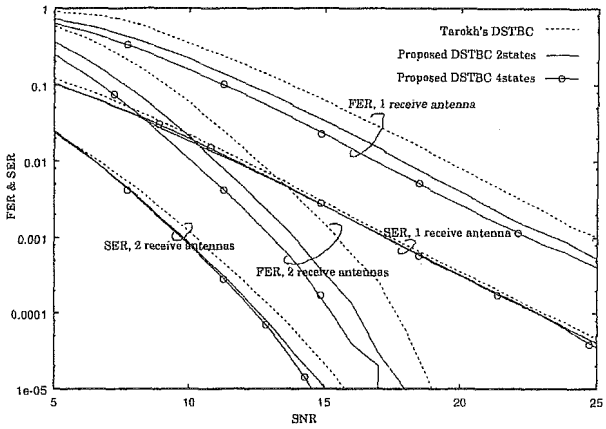

Fig. 9 Frame & symbol error probability for BPSK.

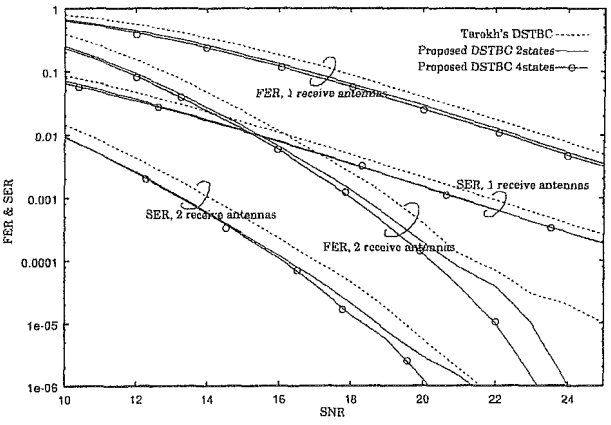

Fig. 10 Frame & symbol error probability for QPSK.

4.2 Simulation Results

Computer simulation performances are given in this section. Note again that we consider a Rayleigh flat fading channel whose path gain is constant during one frame and vary independently from one frame to another. The frame length is 130 symbols. The frame error probability (FER) and the symbol error probability (SER) are shown in Fig. 9–Fig. 11.

In view of the results of FER, Fig. 9 shows the frame error probability of proposed coded DSTBC and Tarokh's DSTBC for BPSK. Exploiting both one receive antenna and two receive antennas, we can confirm that our proposed codes outperforms around 2 dB with two-state code, and 3 dB with four-state code. Additionally, the diversity gain is also achieved. For QPSK in Fig. 10, even though the coding gain is not the maximum for two-state code, it is still larger than that of Tarokh's DSTBC. Two-state code performs around 1 dB better and four state code performs 1.5 dB better, which achieves the maximum coding gain. Due to the small symbol distance, for 8PSK, we only can

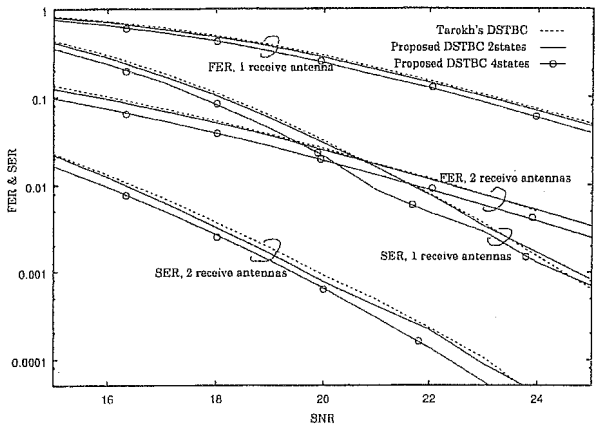

Fig. 11 Frame & symbol error probability for 8PSK.

achieve above 0.5 dB better code with four-state (Fig. 11). Moreover, the improved eight-state and sixteen-state code do not have enough coding gain to have better FER. They performs almost the same or slightly better but is not significant. Considering the tradeoff between system performance and decoding complexity, four-state code can be considered to be the optimum code for 8PSK.

Since our proposal is designed so as to enlarge the path metric considering the whole frame, the FER performs well as we expected. The SER is also shown in Fig. 9–Fig. 11. SER of proposed code also outperforms the conventional DSTBC, however, the improvement is not significant as that of FER.

5. Conclusion

We proposed a coded DSTBC scheme integrated with trellis code based on Tarokh's DSTBC scheme. In order to avoid catastrophic code, our codes are designed so as to increase the number of transmit symbol sets. In addition, set partitioning is also constructed to obtain larger coding gain. It can be seen that the proposed codes outperform Tarokh's DSTBC without an outer code by 1 to 3 dB. Tarokh's DSTBC probably results in a better performance when concatenated with an iterative outer code. However, when we additionally concatenate an outer code with our proposal, it can possibly reduce the number of iterations for an expected BER or FER.

As future works, systematic designs for a larger number of transmit antennas and analysis of the system performance when concatenated codes are used, will be investigated.

References

[1] S.M. Alamouti, "A simple transmit diversity technique for wireless communications," IEEE J. Sel. Areas Commun., vol.16, no.8, pp.1451–1458, Oct. 1998.

[2] V. Tarokh, N. Seshadri, and A.R. Calderbank, "Space-time codes for high data rate wireless communication: Performance criterion and code construction," IEEE Trans. Inf. Theory, vol.44, no.2, pp.744–765, March 1998.

[3] T. Jung and K. Cheun, "Design of concatenated space-time block codes using signal space diversity and the Alamouti scheme," IEEE Commun. Lett., vol.7, no.7, pp.329–331, July 2003.

[4] S. Barbarossa, G. Scutari, and G. Paccapeli, "Concatenated space-time block coding with maximum diversity gain," ICC 2003, vol.3, pp.2129–2133, May 2003.

[5] Y. Gong and K.B. Letaief, "Concatenated space-time block coding with trellis coded modulation in fading channels," IEEE Trans. Wirel. Commun., vol.1, no.4, pp.580–590, Oct. 2002.

[6] B.M. Hochwald and W. Sweldens, "Differtial unitary space-time modulation," IEEE Trans. Commun., vol.48, no.12, pp.2041–2052, Dec. 2000.

[7] B.L. Hughes, "Differential space-time modulation," IEEE Trans. Inf. Theory, vol.46, no.7, pp.2567–2578, Nov. 2000.

[8] V. Tarokh and H. Jafarkhani, "A differential detection scheme for transmit diversity," IEEE J. Sel. Areas Commun., vol.18, no.7, pp.1169–1174, July 2000.

[9] H. Jafarkhani and V. Tarokh, "Multiple transmit antenna differential detection from generalized orthogonal designs," IEEE Trans. Inf. Theory, vol.47, no.6, pp.2626–2631, Sept. 2001.

[10] A. Steiner, M. Peleg, and S. Shamai, "Turbo coded space-time unitary matrix differetial modulation," VTC 2001 Spring, IEEE VTS 53rd, vol.2, pp.1352–1356, May 2001.

[11] J. Suh and M.K. Howlader, "Concatenation of turbo codes to space-time block codes with no channel estimation," MILCOM 2002, Proc., pp.726–731, Oct. 2002.

[12] L.H.-J. Lamp, R. Schober, and R.F.H. Fischer, "Coded differential space-time modulation for flat fading channels," IEEE Trans. Wirel. Commun., vol.2, no.3, pp.582–590, May 2003.

[13] J.P.K. Chu and P.J. Mclane, "Serial concatenation of STBC or dSTBC with convolutional codes or turbo codes for space-time correlated channels," WCNC, 2004, IEEE, vol.3, pp.1764–1769, March 2004.

[14] P. Tarasak and V.K. Bhargava, "Analysis and design Criteria for trellis-coded modulation with differential space-time transmit diversity," IEEE Trans. Wirel. Commun., vol.3, no.5, pp.1374–1378, Sept. 2004.

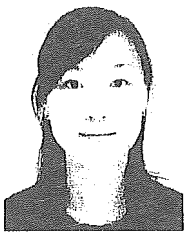

Susu Jiang was born in Jilin, China, in 1979. She received the B.E. and M.S. degrees in electrical and computer engineering from Yokohama National University, Yokohama, Japan, in 2001 and 2003, respectively. She is currently working toward the Ph.D. degree in electrical and computer engineering at Yokohama National University, Yokohama, Japan. Her research interests include space-time coding, channel coding in wireless communications, and information theory. She is a student member of IEEE.

Kentaro Ikemoto was born in Saitama, Japan, in 1976. He received the B.S., M.S., and Ph.D. degrees in electronic and computer engineering from Yokohama National University, Yokohama, Japan, in 2000, 2002 and 2005, respectively. He is currently working toward the research associate with Dr. Anthony Ephremides in Institute for Systems Research from University Maryland, USA. His research interests include adaptive channel coding, space time coding and network coding in wireless communications. He is a member of IEEE.

Ryuji Kohno received the Ph.D. degree from the University of Tokyo in 1984. Dr. Kohno is currently a Professor of the Division of Physics, Electrical and Computer Engineering, Yokohama National University. In his career he was a director of Advanced Telecommunications Laboratory of SONY CSL during 1998–2002 and currently a director of UWB Technology institute of National Institute of Information and Communications Technology (NICT). In his academic activities, he was elected as a member of the Board of Governors of IEEE Information Theory (IT) Society in 2000 and 2003. He has played a role of an editor of the IEEE Transactions on IT, Communications, and Intelligent Transport Systems (ITS). He is a vice-president of Engineering Sciences Society of IEICE and has been the Chairman of the IEICE Technical Committee on Spread Spectrum Technology, that on ITS, and that on Software Defined Radio (SDR). Prof. Kohno has contributed for organizing many international conferences, such as an chair-in honor of 2002 & 2003 International Conference of SDR (SDR'02 & SDR'03), a TPC co-chair of 2003 International Workshop on UWB Systems (IWUWBS'03), and a general co-chair of 2003 IEEE International Symposium on IT (ISIT'03), that of Joint UWBST & IWUWB'04 and so on. He was awarded IEICE Greatest Contribution Award and NTT DoCoMo Mobile Science Award in 1999 and 2002, respectively.

Performance of Super-Orthogonal Convolutional Coding for Ultra-Wideband Systems in Multipath and Multiuser Channels

Tomoko Matsumoto and Ryuji Kohno
Division of Electrical and Computer Engineering, Yokohama National University
79–5 Tokiwadai, Hodogaya, Yokohama, 240–8501, JAPAN.
Tel: +81-45-339-4116, Fax: +81-45-338-1176
E–mail: tomoko@kohnolab.dnj.ynu.ac.jp, kohno@ynu.ac.jp

Abstract—**This paper investigates the application of low-rate error correction codes to ultra-wideband (UWB) systems. Among low-rate channel codes, we focus on the super-orthogonal convolutional codes (SOCC), which have high error correction capability and relatively low implementation complexity with large spreading factor. The performance is analyzed in realistic UWB channels containing multiuser interference (MUI) and inter-symbol interference (ISI) assuming coherent RAKE receiver followed by matched filter (MF) receiver. Two types of combining schemes, maximum-ratio combining (MRC) and minimum mean-squared error (MMSE) combining schemes, are considered. The performance is compared with conventional higher rate convolutional codede schemes in terms of bit error probability under the constraint that the total spreading factor is fixed. The results show that the SO convolutional coded scheme outperforms the conventional higher-rate convolutional codeed schemes for both types of receivers.**

Index Terms—**super-orthogonal convolutional codes, ultra-wideband, code-spreading, coherent RAKE combining**

1. INTRODUCTION

In recent years, ultra-wideband (UWB) technology is expected to serve as a core physical layer technology for short and medium range communications. The potential applications of UWB technology include high data rate wireless personal area networks (WPANs), which can achieve more than 100Mbps over short distance. The alternative application is low-rate WPANs for low data rate, low cost applications combined with precise ranging and positioning capabilities. Due to the large bandwidth, however, UWB systems need to coexist with other exsisting systems. In order to reduce the intra-system interference, UWB devices must meet stringent power spectral density (PSD) requirements specified by regulations. This highlights the importance of power efficiency in the design of a UWB system. Therefore, the application of strong forward error control (FEC) codes is neccessary.

With its spread spectrum nature, UWB systems can obtain highly reliable transmission at the expense of bandwidth expansion by low-rate coding [1]. In fact, the low-rate codes have been applied to spread-spectrum (SS) systems like IS-95, because bandwidth expansion by coding is utilized as spreading gain. It is known that an appropriate allocation of total bandwidth expansion between coding and spreading can drastically increase the system capacity. Based on this fact, the application of SOCC to a time-hopping (TH) based UWB has been studied in [2] so far. The SOCC is a family of very low-rate orthogonal convolutional codes (VLOCC) introduced in [3] by Viterbi et al. The results in [2] demonstrated that the SO coded system outperform the uncoded system in multiuser AWGN channel. However, neither the comparison between SOCC and other channel codes nor performance analysis under fading channel has been done.

In this paper, the performance is analyzed in realistic UWB channels containing multiuser interference (MUI) and inter-symbol interference (ISI) assuming coherent RAKE receiver followed by matched filter (MF) receiver. Two types of combining schemes, maximum-ratio combining (MRC) and minimum mean-squared error (MMSE) combining schemes, are considered. The performance is compared with conventional higher rate convolutional coded schemes in terms of bit error probability under the constraint that the total spreading factor is fixed. The results demonstrate that with short code spreading, the performance of SO coded scheme degrades due to the poor correlation property of the spreading sequence. On the contrary, comined SOCC and code-hopping scheme, instead of short code spreading, outperforms the conventional higher rate convolutional coded scheme under multipath and multiuser environment for both types of receivers.

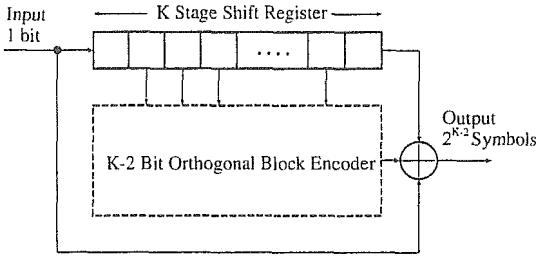

Figure 1: Encoder for SOCC of arbitrary constraint length K.

2. SYSTEM DESCRIPTION

2.1. The Super-Orthogonal Convolutional Codes

The SOCC is a family of VLROCC proposed by Viterbi et al. [3]. The codewords for SOCC are given by Walsh-Hadamard matrices,

$$H_k = \begin{pmatrix} H_{k-1} & H_{k-1} \\ H_{k-1} & \overline{H}_{k-1} \end{pmatrix}, \quad H_1 = 0. \tag{1}$$

where k is an positive integer. This yields length 2^k codewords and the resultant code rate is 2^{-k}. Fig. 1 illustrates a encoder for SOCC with arbitrary constraint length K. The encoder has a shift register of length K. In the K bit shift register, the $K-2$ bit memories in the middle drive a $(K-2)$ bit block orthogonal encoder which determines one of 2^{K-2} orthogonal (i.e., Walsh-Hadamard) sequences of length 2^{K-2}. Finally, the remaining two outer memories are both added by modulo-2 to every one of 2^{K-2} Walsh-Hadamard sequence. The resultant codes are called *super-orthogonal convolutional codes* of code rate $r = 2^{-K+2}$.

2.2. Transmit Signal

The overall system model considered is illustrated in Fig. 2. At the transmitter, a information stream $\boldsymbol{d}_k \in \{0,1\}$ is encoded by a convolutional encoder, where subscript k denotes the kth user. The resulting stream of binary code word $\boldsymbol{b}_k \in \{0,1\}$ is

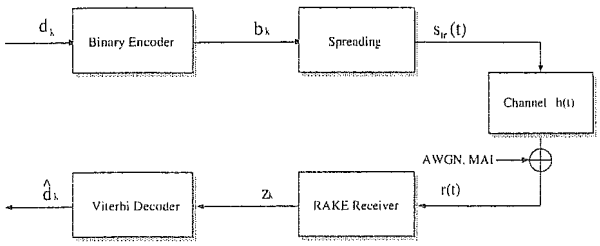

Figure 2: Transmitter model

then spread by user specific spreading sequence. The transmit signal for the kth user of is given by

$$s_{tr}^{k}(t) = \sum_{j=-\infty}^{\infty} (2b_k(j) - 1)\, \tilde{s}_{k,j}(t - jT_s) \tag{2}$$

where index j stands for the symbol number, $b_k(j)$ is a coded data bit corresponding to the jth symbol. Throughout the paper, we consider binary phase shift keying (BPSK) for modulation scheme. The signature waveform of duration T_s is given by

$$\tilde{s}_{k,j}(t) = \sqrt{\frac{E_s}{N_c}} \sum_{n=0}^{N_c-1} c_{k,n}(j) w_{tr}(t - nT_c) \tag{3}$$

where E_s denotes symbol energy, and transmit pulse waveform $w_{tr}(t)$ with duration T_p is assumed to have a unit energy. The pulse width is assumed to be less than the chip duration T_c, i.e., $T_p < T_c$. In addition, we assume $T_s = N_c T_c$. Let $\boldsymbol{c}_k(j) = [c_{k,0}(j), c_{k,1}(j), \cdots, c_{k,N_c-1}(j)]^T$ denote the spreading sequence for jth symbol. Since we assume direct-sequence (DS) spreading, $\boldsymbol{c}_k \in \{\pm 1\}$. If the same sequence is used for each symbol, $\boldsymbol{c}_k(j) = \boldsymbol{c}_k$. However, note that we employ code-hopping scheme, whereby several spreading sequence are used per single user and they are switched between a predetermined set of sequences. This results in the different interference from one symbol to another and make the interference probability density function from other users close to Gaussian distribution. We define the number of pre-determined sequence per single user as J. Let $\boldsymbol{a}_k = [\boldsymbol{a}_k(0), \boldsymbol{a}_k(1), \cdots, \boldsymbol{a}_k(J-1)]$ be a set of sequence for the kth user. Then the sequence is switched such that $\boldsymbol{c}_k(j) = \boldsymbol{a}_k(j \bmod J)$.

2.3. Received Signal

The received signal for the kth user can be expressed as

$$\begin{aligned} s_{rec}^{k}(t) &= h_k(t) * s_{tr}^{k}(t) \\ &= \sum_{l=1}^{L_p} \alpha_l^k \tilde{p}_{k,j}(t - nT_s - \tau_l), \end{aligned} \tag{4}$$

where $h_k(t)$ is the channel impulse response for the kth user, and $(*)$ stands for convolution. $\tilde{p_k}(t)$ stands for the received signature waveform given by

$$\tilde{p}_{k,j}(t) = \sqrt{\frac{E_s}{N_c}} \sum_{n=0}^{N_c-1} c_{k,n}(j) w_{rec}(t - nT_c) \tag{5}$$

where $w_{rec}(t)$ represents the received pulse shape. In this paper, we assume that the received pulse waveform is second-derivative of transmit waveform [5]. It should be also noted that the receiver knows the received pulse shape so as to correlate received signal with template waveform matched to received pulse waveform. This paper is written based on the assumption that the channel is to follow Saleh-Valenzuela (SV) model proposed by the IEEE 802.15 TG3a, e.g., CM1-CM4 [6], where the channel impulse response is given by

$$h_k(t) = \sum_{l=1}^{L_p} \alpha_l^k \delta(t - \tau_l), \tag{6}$$

where α_l^k and τ_l is the channel coefficient and the delay time of the lth multipath component of kth user respectively, L_p is the maximum number of multipath component. Note that the total energy of $h_k(t)$ is normalized. Assuming that N_u transmitters are active, then the total received signal is represented as follows.

$$r(t) = \sum_{k=1}^{N_u} A_k s_{rec}^{k}(t - \tau_k) + n(t) \tag{7}$$

in which A_k and τ_k are the channel attenuation and relative time offset between transmitted signal of the kth user and receiver of the desired user. Without loss of generality, we assume desired user is user 1. Finally, $n(t)$ is additive white Gaussian noise (AWGN) with zero mean and variance σ_n^2.

2.4. RAKE Receiver Structure

In this paper, a coherent RAKE receiver followed by matched filter (MF) is considered to exploit multipath diversity and combat fading. With hundreds of multipath components in UWB channel, it is too expensive to gather all of the multipath component. Thus, we adopt a suboptimum method called selective-RAKE, where only the largest L paths out of L_p paths are combined. Fig. 3 illustrates a RAKE receiver structure considered in this paper. As shown in Fig. 3, the receiver consists of a bank of L RAKE fingers, each correlating to a different delay of the received signal. In order to make theoretical analysis tractable, the following assumptions are made. First, the synchronization between transmitter and receiver for desired user is perfectly established, i.e, $\tau_1 = 0$. Second, and receiver can perfectly estimate the channel response for the desired user $h_1(t)$ prior to data transmission by using some pilot symbols while the receiver know neither arrival timing τ_k nor channel response $h_k(t)$ for other interference users ($k \neq 1$).

Let λ_l and θ_l for $0 < l \leq L$ denote the estimated amplitude and delay of the L-largest multipaths. We further assume that the delays are ordered (i.e., $\theta_1 < \theta_2 < \cdots < \theta_L$). In what follows, we focus on desired user 1 and so the subscript k is dropped. Let $\boldsymbol{y}(j)$ denote a matched filter (MF) output associated with jth symbol given by $\boldsymbol{y}(j) = [y_1(j), y_2(j), \cdots, y_L(j)]^T$ where $y_l(j)$ denotes the MF output corresponds to the lth multipath given by

$$y_l(j) = \int_0^{T_s} r(t - jT_s - \theta_l) \cdot \tilde{p_1}(t) dt \tag{8}$$

The MF outputs are then combined to form decision statistics $z(j)$. Let $\boldsymbol{w}(j) = [w_1(j), w_2(j), \cdots, w_L(j)]^T$ denote a combining weight for jth symbol, then the decision statistic corresponding to the jth symbol is given by

$$z(j) = \boldsymbol{w}^T(j)\boldsymbol{y}(j). \tag{9}$$

By using (9), the metric is calculated and decoding is performed by Viterbi algorithm.

3. Performance Analysis

3.1. Derivation of Combining Weight

In this paper, we consider two types of RAKE combining schemes, that is, MRC and MMSE combining receivers. MRC is known to be optimum under the AWGN channel, but not in

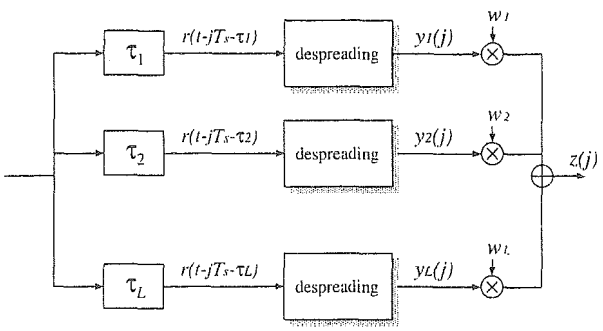

Figure 3: RAKE receiver structure

other cases. On the contrary, MMSE combining has a capability to effectively suppress the interference from other users.

Since the correlator output is composed of sum of the signal components of all users, (2-D) can be written as

$$\boldsymbol{y}(j) = \sum_{k=1}^{N_u} \boldsymbol{G}_k(j)\boldsymbol{b}_k(j) + \tilde{\boldsymbol{n}}(j). \tag{10}$$

where, a length N_a vector $\boldsymbol{b}_k \in \{\pm 1\}$ denotes the data bit for the kth user, $\tilde{\boldsymbol{n}}(j) = [\tilde{n_1}(j), \tilde{n_2}(j), \cdots, \tilde{n_L}(j)]$ represents noise term after despread as

$$\tilde{n_l}(j) = \int_0^{T_s} n(t - jT_s - \theta_l)\tilde{p_1}(t)dt. \tag{11}$$

In (10), $\boldsymbol{G}_k(j)$ is a L-by-N_a matrix, where N_a is maximum number of symbols in a observation time $T_w = \theta_L - \theta_1 + T_s$. In more detail, N_a can be expressed as $N_a = N_l + N_r$, where $N_l = \lceil T_{max}/T_s \rceil$, $N_r = \lceil T_w/T_s \rceil$, where T_{max} denotes the maximum delay spread. Let $\boldsymbol{G}_k(j) = \left[\boldsymbol{g}_1^k(j), \cdots, \boldsymbol{g}_{N_a}^k(j)\right]$ and $\boldsymbol{g}_i^k(j) = \left[g_{i,1}^k, \cdots, g_{i,L}^k\right]^T$ represents length L interference coefficient vector from ath symbol of the kth user. Note that when $k = 1$ and $i = N_l$, $\boldsymbol{g}_i^k$ represents the desired user's output. Thus, each component of $\boldsymbol{g}_i^k(j)$ is expressed as

$$g_{i,l}^k(j) = \sum_{m=1}^{L_p} \alpha_m^k R_{1,k}\left(\tau_m^k + (i - N_l)T_s - \tau_l^1\right) \tag{12}$$

where $\tau_l^k = \tau_k + \tau_l$ for all k and l, $R_{u,v}(x)$ denotes the cross-correlation function between $\tilde{p_u}(x)$ and $\tilde{p_v}(x)$

$$R_{u,v}(x) = \int_0^{T_s} \tilde{p_u}(t)\tilde{p_v}(t + x)dt \tag{13}$$

Here let us define a correlation matrix of (10) as follows.

$$\boldsymbol{R}(j) = \mathrm{E}\left[\boldsymbol{y}(j)\boldsymbol{y}^T(j)\right] \tag{14}$$

$$= \sum_{k=1}^{N_u} \boldsymbol{G}_k\boldsymbol{G}_k^T + \sigma_n^2\boldsymbol{I}_L \tag{15}$$

where, $\mathrm{E}[\cdot]$ denotes mathematical expectation, $\boldsymbol{I}_L$ denotes a L-by-L identity matrix. In case of short-code spreading case, $\boldsymbol{R}(j) = \boldsymbol{R}$. In case of code-hopping scheme, we need to calculate $\boldsymbol{R}(j)$ and $\boldsymbol{w}(j)$ for $0 \le j < J$. Based on the MMSE criterion, the optimum filter weight for MMSE combining case converges into the following solution.

$$\boldsymbol{w}(j) = \arg\min_{\boldsymbol{w}} \mathrm{E}\left[\left(\boldsymbol{w}^T(j)\boldsymbol{y}_l(j) - d_1(j)\right)^2\right]$$

$$= \boldsymbol{R}^{-1}(j)\boldsymbol{p}(j) \tag{16}$$

Table 1: Convolutional codes parameters.

Scheme	CC 1	CC 2	SOCC
Constraint length (K)	5		
Code rate (r)	1/2	1/4	1/8
Generators	$(23,35)_8$	$(25,27,33,37)_8$	-
Free distance (d_f)	7	16	64
Sequence length (N_c)	127	63	31
Total processing gain	254	252	248

where $\boldsymbol{p}(j) = \mathrm{E}\left[\boldsymbol{y}(j)d_1(j)\right]$. For the case of MRC, the weight is simply

$$\boldsymbol{w}(j) = \boldsymbol{\alpha}_1 \tag{17}$$

where $\boldsymbol{\alpha}_k = \left[\alpha_1^k, \cdots, \alpha_L^k\right]^T$.

3.2. SINR Derivation

We derive signal-to-interference plus noise ratio (SINR) to derive the bit error rate. In this paper, in order to simplify the analysis, MUI and ISI are both assumed to be Gaussian distribution. By using the weight derived in the (16) and (17), the SINR per symbol at the output of the RAKE receiver for both MRC and MMSE combining can easily written as

$$\mathrm{SINR}(j) = \frac{\boldsymbol{w}^T(j)\boldsymbol{R}_s(j)\boldsymbol{w}(j)}{\boldsymbol{w}^T(j)\boldsymbol{R}_I(j)\boldsymbol{w}(j)}, \tag{18}$$

where $\boldsymbol{R}_s(j) = \boldsymbol{g}_{1,N_l}^T(j)\boldsymbol{g}_{1,N_l}(j)$ and $\boldsymbol{R}_I(j) = \boldsymbol{R}(j) - \boldsymbol{R}_s(j)$ denote correlation matrix for desired output and that for total interference, respectively. When using multiple spreading sequence, each SINR is averaged as

$$\overline{\mathrm{SINR}} = \frac{1}{J}\sum_{j=0}^{J-1} \mathrm{SINR}(j) \tag{19}$$

3.3. Upper Bound of Bit Error Probability

The upper bound of BER of any convolutional codes can be obtained from the generating function $T(X, Y)$. The union bound of the BER is given by [4]

$$P_b < \frac{1}{k}\frac{dT(X,Y)}{dY}\Big|_{Y=1} \tag{20}$$

$$= \frac{1}{k}\sum_{d=d_f}^{\infty} B_d X^d \tag{21}$$

where $X = \exp(-\gamma_s)$, and γ_s denotes signal-to-noise ratio per symbol. Here the SINR derived in Eq. (18) is a function of $\boldsymbol{\alpha} = [\boldsymbol{\alpha}_1, \boldsymbol{\alpha}_2, \cdots, \boldsymbol{\alpha}_{N_u}]$ and $\boldsymbol{\tau} = [\tau_1, \tau_2, \cdots, \tau_{N_u}]$. Because SV model is not stochastic model, it is hard to obtain exact solution of average bit error probability. Thus, we calculate it by numerical integration as follows.

$$\bar{P_b} = \int\int (P_b|\boldsymbol{\alpha}, \boldsymbol{\tau})d\boldsymbol{\alpha}d\boldsymbol{\tau}. \tag{22}$$

4. Numerical Results

In this section, the bit error performance of SO coded scheme is compared with the other convolutional coded coded scheme based on computer simulations.

4.1. Simulation Parameters

Table 1 shows convolutional codes parameters. As shown in Table 1, we consider three types of convolutional codes, that is, convolutional code (CC) of rate 1/2 and 1/4, and SOCC. For each codes, two different constraint length, $K = 5$ and $K = 6$, are considered. Note that for SOCC, code rate is 1/8 for $K = 5$